의학박사 학위논문

# Studies on the proliferation of microglia and reduction of amyloid plaque burden in the brain by chronic infection with *Toxoplasma gondii* in Alzheimer's disease model mice

알츠하이머병 모델 마우스에서 톡소포자충의
만성 감염이 유도하는 뇌 내의 미세아교세포 증식과
아밀로이드 플라크 부하 감소에 관한 연구

2021년 8월

서울대학교 대학원
의학과 열대의학전공
신 지 훈

# Studies on the proliferation of microglia and reduction of amyloid plaque burden in the brain by chronic infection with *Toxoplasma gondii* in Alzheimer's disease model mice

지도교수 신 은 희

이 논문을 의학박사 학위논문으로 제출함

2021년 4월

서울대학교 대학원
의학과 열대의학전공
신 지 훈

신지훈의 의학박사 학위논문을 인준함

2021년 7월

| | |
|---|---|
| 위 원 장 | 최 민 호 |
| 부위원장 | 신 은 희 |
| 위 원 | 박 현 |
| 위 원 | 장 은 화 |
| 위 원 | 송 현 범 |

# Studies on the proliferation of microglia and reduction of amyloid plaque burden in the brain by chronic infection with *Toxoplasma gondii* in Alzheimer's disease model mice

**by**
**Ji-Hun Shin**
**(Directed by Prof. Eun-Hee Shin)**

A thesis submitted in partial fulfillment of the requirements for
the degree of Doctor of Philosophy in Medicine
(Major in Tropical Medicine and Parasitology)
at Seoul National University College of Medicine

**July 2021**

**Doctoral Committee:**

| | | |
|---|---|---|
| **Professor** | Min Ho Choi | **Chairman** |
| **Professor** | Eun Hee Shin | **Vice chairman** |
| **Professor** | Park Hyun | |
| **Professor** | Zhang Yin Hua | |
| **Professor** | Hyun Beom Song | |

# ABSTRACT

## Studies on the proliferation of microglia and reduction of amyloid plaque burden in the brain by chronic infection with *Toxoplasma gondii* in Alzheimer's disease model mice

**Ji-Hun Shin**
Department of Tropical Medicine and Parasitology,
Seoul National University College of Medicine

Alzheimer's disease (AD) is known to progressively worsen with an accumulation of amyloid β (Aβ) plaques in the brain. A recent study has showed that chronic *Toxoplasma gondii* infection reduces the amyloid plaque burden in a mouse model of Alzheimer's disease (AD). The release of *T. gondii*-induced anti-inflammatory cytokines (transforming growth factor-beta and interleukin-10) and elevated Ly6C$^{hi}$ monocyte levels are suggested to be the underlying mechanisms. It is well acknowldeged that microglial phagocytosis is important to eliminate amyloid plaque in AD. Until recently, the microglial proliferation and the mechanistic links to amyloid plaque burden reduction and AD pathology following *T. gondii*-infection is not clear. The aim of the study is to investigate the role of *T. gondii* infection in the microglial proliferation and phenotype changes on amyloid plaque reduction using 5XFAD transgenic mice and compared the results with control mice.

Results showed that, in the normal mouse brain, the number of Iba1-positive microglia and TMEM119-positive resident homeostatic microglia was significantly increased during 3 to 36 weeks of *T. gondii* infection period,

expressing Ki67 proliferation marker. Microarray analysis of microglial markers (*Iba1*, *P2ry13*, *Cx3cr1*, *Tmem119*) and trophic factors (*Il1β*, *Tnfα*, *Mcsf*, *NFκB1*) were consistent with microglial proliferation. Next, I have analyzed the association between microglial proliferation and the Aβ plaque burden in brain tissues isolated from 5XFAD AD mice (AD group) and *T. gondii*-infected AD mice (AD + Toxo group). Compared with the AD group, the AD + Toxo group showed a significantly reduced Aβ plaque burden but significantly higher homeostatic microglial proliferation and increased numbers of plaque-associated microglia following 10 months post- *T. gondii* infection. Microarray analysis showe that microglial markers (*Iba1*, *P2ry13*, *Tmem119*), trophic factors (*Tnfα*, *Il1β*) was increased in the AD+Toxo group, and enzyme-linked immunosorbent assay result of Aβ peptide was significantly decreased in the AD+Toxo group as the result of amyloid plaque counting. Most plaque-associated microglia were transformed into the TREM2-positive and Lpl-positive disease-associated microglia (DAM) phenotypes in both AD and AD + Toxo groups and underwent apoptosis after lysosomal degradation of phagocytosed Aβ plaques, which highlights that a sustained supply of homeostatic microglia is necessary to reduce the Aβ plaque burden.

Through this study, I discovered that chronic *T. gondii* infection could induce microglial proliferation in the brains of mice with progressive AD and the sustained supply of homeostatic microglia may be a promising therapeutic approach against AD.

*This dissertation is based on the previously published article (Shin et al., 2021).

**Keyword:** *Toxoplasma gondii*, Chronic infection, Homeostatic microglia, Alzheimer's disease, 5XFAD mouse, Disease-associated microglia

**Student Number: 2015-21959**

# CONTENTS

# LIST OF FIGURES

## Study I: Changes in the proliferation of microglia induced by chronically infected *Toxoplasma gondii*

**Study II: Effects of *Toxoplasma gondii* infection on amyloid plaque burden in 5XFAD Alzheimer's disease mouse model**

# LIST OF TABLES

# LIST OF ABBREVIATIONS

| | |
|---|---|
| CNS | Central nervous system |
| AD | Alzheimer's disease |
| DAM | Disease-associated microglia |
| SOCS1 | Suppressor of cytokine signaling 1 |
| Arg1 | Arginase 1 |
| pSTAT1 | Phosphorylation of signal transducer and activator of transcription 1 |
| PCR | Polymerase chain reaction |
| DNA | Deoxyribonucleic acid |
| RNA | Ribonucleic acid |
| H&E | Hematoxylin and eosin |
| IHC | Immunohistochemistry |
| PBS | Phosphate buffered saline |
| Aβ | Amyloid beta |
| IFA | Immunofluorescence assay |
| MFI | Mean fluorescence intensity |
| PI | Post-infection |
| TUNEL | Terminal deoxynucleotidyl transferase dUTP nick end labeling |

# INTRODUCTION

Microglia are resident macrophages of the central nervous system (CNS) that constitute 5–10% of total brain cells, maintain CNS homeostasis, and protect the CNS by phagocytosing pathogens (Frost and Schafer, 2016; Chen and Trapp, 2016; Galloway et al., 2019; Ginhoux and Garel, 2018). Microglial heterogeneity, defined with key regulators, markers, and drug targets, is categorized by homeostatic, pro-inflammatory, and anti-inflammatory microglial subtypes (Rangaraju et al., 2018). In addition, microglia play important disease-modifying roles in neurodegenerative diseases, including Alzheimer's disease (AD), as innate immune cells of the CNS (Rangaraju et al., 2018; Keren-Shaul et al., 2017; Deczkowska et al., 2018). Transcriptome studies have indicated that homeostatic microglia gradually adopt a unique phagocytic disease-associated microglia (DAM) phenotype in neurodegenerative disease, chronic inflammation, and advanced aging (Rangaraju et al., 2018). Recent studies have also characterized the phenotype of homeostatic microglia and DAM with specific markers. For example, transmembrane protein 119 (TMEM119) has been identified as a specific marker for brain-resident homeostatic microglia (Bennett et al., 2016; Keren-Shaul et al., 2017), whereas the DAM phenotype showed a loss of homeostatic gene signature with neurodegeneration in AD (Sobue et al., 2021). DAM microglia have been characterized by the upregulation of TREM2 (Triggering Receptor Expressed on Myeloid Cells 2)-dependent genes and lipid metabolism genes (TREM2, Lpl, Cst7) (Keren-Shaul et al., 2017; Griciuc and Tanzi, 2021). By contrast, researchers have not yet determined the effects of microbial pathogens, which induce microglial proliferation, on AD

progression using the CNS infection model; in addition, detailed studies on the effect of microbial infection in advanced AD are limited.

*Toxoplasma gondii*, a protozoan parasite that commonly infects humans and animals, chronically infects the brain, which acquires immunity against toxoplasmosis (Jung et al., 2012; Hwang et al., 2018). In the brain, *T. gondii* infection induces the expression of anti-inflammatory cytokines and negative regulators of toxoplasmic encephalitis, namely suppressors of cytokine signaling 1 (SOCS1) and Arg1, to reduce the inflammatory response (Jung et al., 2012; Hwang et al., 2018). Through a series of immunomodulatory processes, microglia increase significantly from 3 to 9 weeks after *T. gondii* infection and slightly decrease after nine weeks (Hwang et al., 2018). In previous studies, neuroinflammation was suppressed, and homeostasis was restored by increasing anti-inflammatory cytokine production in the disease-associated inflammatory response state (Jung et al., 2012; Hwang et al., 2018). However, the proliferation and role of microglia in chronic *T. gondii* infection have not been discussed sufficiently. Considering that microglia continuously monitor the surrounding parenchyma to sense alterations in brain function and are involved in controlling neuronal excitability, synaptic activity, neurogenesis, and clearance of apoptotic cells in the healthy adult brain (Lauro and Limatola, 2020), it would be interesting to determine how microglia affect chronic neurodegenerative diseases, such as AD, after *T. gondii* infection.

Microglia are categorized by their phenotypes in health or disease states (Frost and Schafer, 2016; Chen and Trapp, 2016; Galloway et al., 2019; Ginhoux and Garel, 2018; Rangaraju et al., 2018; Keren-Shaul et al., 2017; Deczkowska et al., 2018;

Lauro and Limatola, 2020). Microglial function in the normal brain has been described as surveillance and limiting the over-production of neurons and excitatory synapses through microglia-mediated phagocytosis to maintain homeostasis (Chen and Trapp, 2016). However, microglia are activated by acute insults and chronic disease states; reactive microglia are motile and destructive as they physically surround or target specific structures, such as dying cells, neurons, dendrites, blood vessels, and amyloid plaques, and therefore defend against CNS diseases (Chen and Trapp, 2016). In *T. gondii* infection, the microglial phenotype is significant for the disease-associated immune response (Hwang et al., 2018). *T. gondii* infection induces M1 polarization of microglia while reducing detrimental inflammatory immune responses through the induction of SOCS1, reducing the phosphorylation of signal transducer and activator of transcription 1 (pSTAT1), and the induction of anti-inflammatory cytokines (Hwang et al., 2018). In addition, the immune environment induced by *T. gondii* infection in the CNS has been determined to play a role in the inhibition of neurodegeneration and clearance of β-amyloid plaques in Tg2576 AD mice (Jung et al., 2012). Furthermore, the researchers who studied the effect of amyloid plaque reduction to determine whether the effect is due to a strain-specific result found that only the reduction induced by avirulent type II strain can induce amyloid plaque reduction in AD model mice (Cabral et al., 2017). Nevertheless, little is known regarding the functional role of *T. gondii*-induced microglial proliferation in AD pathology. In other words, the role of *T. gondii*-induced microglial proliferation in the phagocytosis of β-amyloid plaques has not yet been reported.

The 5XFAD mouse, an experimental animal model of early-onset AD, in which β-amyloid plaques are first observed at two months of age, and cognitive deficits are observed at 4–6 months, is used to study the age-dependent progression of AD-like pathology (Lee and Han, 2013). *T. gondii* infection ameliorated β-amyloidosis by activating the immune response, including increased amyloid-β (Aβ) phagocytosis by $Ly6C^{hi}$ monocytes, on day 28 after *T. gondii* infection in 8-week-old 5XFAD mice (Möhle et al., 2016). Although the microglial population increased in the brain and microglia were localized to the vicinity of Aβ plaques, the role of microglia received less attention, due to their lower *ex vivo* phagocytic capacity, than $Ly6C^{hi}$ monocytes (Möhle et al., 2016). However, in that study, the infection period of *T. gondii* for the *ex vivo* phagocytic capacity experiment was only one month, which represents the early stage of infection and, thus, is insufficient to evaluate the effects of infection. Considering that *T. gondii* infection persists for a long time in the brain and the pathophysiology of AD is regulated over the long term, the phagocytic role of microglia in the brain has to be observed in mice older than six months with the progression of AD. In that respect, the previous study reported that β-amyloidosis of the brain was reduced at six months after *T. gondii* infection in 9-month-old Tg2576 AD mice; however, at that time, there was no study on the role of microglia in ameliorating AD (Jung et al., 2012). Therefore, in this study, I aimed to elucidate the role of microglia increased after *T. gondii* infection in reducing the amyloid burden in a 5XFAD transgenic mouse model. As the basis of this study, I already demonstrated that microglia were persistently increased during 12 weeks of chronic infection of *T. gondii* (Hwang and Shin et al., 2018). Accordingly, I designed the

time schedule for this study with the following purposes; whether microglia increase even during 10 months of chronic *T. gondii* infection and the increased microglia can reduce the amyloid burden in 12 months 5XFAD mice. Because the 5XFAD transgenic mouse model exhibits a rapid and massive increase of amyloid deposition from 2 months old to 6 months old (Oakley H et al., 2006), 10 months *T. gondii* infection period (from 2 months after birth) was used to evaluate the overall effect of infection on reducing amyloid burden.

Drug development is very important for therapeutic approaches to AD. Medications for AD provide temporary relief from memory loss and cognitive dysfunctions (Dong et al., 2016) but cannot stop or reverse AD's progression (Dong et al., 2016). Therefore, the discovery of new medications and curative strategies for AD therapy is required. Activated microglia are found surrounding and phagocytosing Aβ plaques; however, they are also implicated in the etiology of AD through oxidative damage and pro-inflammatory signaling (Baik et al., 2016; Wes et al., 2016). Despite differences of opinions in defining the role of activated microglia for treating AD, targeting microglia for treating AD remains an attractive prospect (Dong et al., 2019; Baik et al., 2016; Wes et al., 2016). The goal of a therapeutic approach targeting microglia in AD may be viewed as an attempt to return the spectrum of microglial phenotypes from the disease state (mainly synaptic pruning, reactive oxygen species generation, and inflammatory cytokine production) to the cognitively normal state (mainly trophic support and phagocytosis) (Wes et al., 2016). Therefore, it is important to focus on the biological role of microglial proliferation in *T. gondii*-infected AD model mice. Notably, it had been demonstrated that *T.*

*gondii* infection induces M1 polarization and Th1 inflammatory responses in response to microbial infection but does not induce inflammatory responses through immune regulation during chronic infection (Jung et al., 2012; Hwang et al., 2018; Ham et al., 2020).

Considering that chronic *T. gondii* infection reduced the amyloid burden in aged Tg2576 mice (Jung et al., 2012), the increase in microglial proliferation after *T. gondii* infection may contribute to Aβ clearance (Hwang et al., 2018). Both the activation and phagocytic activity of microglia are important for disease modification in AD. This study highlights the role of microglia in reducing the amyloid burden considering homeostasis and microglial activation, the close association between microglia and Aβ plaques, the switch to the DAM phenotype, and the phagocytic capacity and apoptosis of microglia. Simultaneously, it emphasizes the importance of continuous microglial proliferation as a therapeutic target for AD.

# Materials and Methods

## 1. Ethics statement

All animal experiments were approved by the Institutional Animal Care and Use Committee at Seoul National University (permit number: SNU-110315-5). Mice were maintained in an animal facility according to the standards of the Animal Protection Act and the Laboratory Animal Act in Korea. Mouse experiments were performed according to global standards, such as those established by the Association for Assessment and Accreditation of Laboratory Animal Care International.

## 2. 5XFAD transgenic mice

5XFAD mice (The Jackson Laboratory, Bar Harbor, ME, USA) were provided by Dr. Inhee Mook-Jung at Seoul National University and bred by mating male mice with wild-type females (C57BL6/SJL). Genotyping for confirming the presence of human APP and PSEN1 transgenes was performed through polymerase chain reaction (PCR) analysis of tail genomic DNA. PCR products (350 bp for APP and 608 bp for PSEN1) were analyzed using 1% agarose gel electrophoresis and detected through ethidium bromide staining. Primer sequences are listed in the Table (Table 1).

## 3. *T. gondii* infection and experimental design

To infect 5XFAD mice, *T. gondii* ME49 cysts were obtained from the brain tissues of C57BL/6 mice (Orient Bio Animal Center, Seongnam, South Korea) infected with

ten cysts. Seven-week-old C57BL/6 mice were infected with ten cysts for the histopathological examination and microarray analysis of the brain at 0, 3, 6, 12, and 36 weeks after infection (n = 2–4 per group). Eight-week-old 5XFAD mice were orally infected with ten cysts and euthanized using $CO_2$ asphyxiation for histopathological examination of the brain at ten months after infection (n = 6).

## 4. Hematoxylin and eosin staining and Congo red staining of the brain tissue

Brain tissues were fixed in 10% formalin and embedded in paraffin after dehydration through an ethanol gradient. Brain tissues, which were coronally sectioned at 10 μm thickness, were stained with Harris' hematoxylin and eosin (H&E) to detect *T. gondii* tissue cysts and neuronal degeneration, indicated by acidophilic neurons in layer V of the cerebral cortex (n = 6 per group). Observations were performed using light microscopy (CKX 41, Olympus, Tokyo, Japan) and a color digital camera (DP72, Olympus). For Congo red staining, sectioned brain tissues were incubated in 0.4% aqueous Congo red solution (Sigma-Aldrich, St Louis, MO) for 10 min at room temperature (RT), counterstained in hematoxylin for 10 min, and dipped in acid alcohol (1% HCl in EtOH) for differentiation. Finally, after the sections were dehydrated and mounted, dense core plaques in the cortex and hippocampus were counted using a color digital camera attached to a light microscope and evaluated using ImageJ (Version 1.45, National Institute of Health, Bethesda, MD, USA).

## 5. Immunohistochemistry

Immunohistochemistry (IHC) was performed after Congo red staining. Briefly, tissue sections were deparaffinized in xylene, rehydrated in a graded series of ethanol, and rinsed with distilled water. After antigen retrieval, endogenous peroxidase activity was blocked using $H_2O_2$ in blocking buffer (1% fetal bovine serum in PBS) for 30 min. Then the slides were incubated with rabbit anti-mouse Iba-1 (Wako, VA, USA) as the primary antibody (Ab) and UltraMap anti-Rb horseradish peroxidase (HRP) (Ventana Medical Systems, Tucson, AZ, USA) as the secondary Ab. The ChromoMap 3,3´-Diaminobenzidine (DAB) detection kit (Ventana Medical System) was used for detecting the DAB signal, and hematoxylin was used for counterstaining. Slides were observed using a light microscope equipped with a color digital camera.

## 6. Immunofluorescence staining and quantitative analysis

Brain sections with antigen retrieval were permeabilized with 0.5% Triton X-100 in phosphate-buffered saline (PBS) for 10 min at RT and blocked in 2% bovine serum albumin (BSA)/PBS or 10% donkey serum for double-staining. Antibodies used for immunofluorescence (IF) staining are listed in Table 2. Samples were stained with the corresponding secondary Ab, and nuclei were stained with 4′,6-diamino-2-phenylindole, dihydrochloride (DAPI; Sigma-Aldrich, St. Louis, MO, USA). For detecting amyloid plaque, methoxy-X04 (Abcam, Pittsburgh, PA, USA) staining was performed before DAPI counterstaining. Tissue sections were stained with 100 μM methoxy-X04 in 40% ethanol (adjusted to pH 10 with 0.1 N NaOH) for 10 min and

then incubated with 0.2% NaOH in 80% ethanol for 2 min. Immunostained slides were observed using fluorescence microscopy (Leica DMI6000B, Wetzlar, Germany). For quantifying the area covered by microglia in the cortex and hippocampus, slides stained with Iba1 and TMEM119 Abs were used for calculating the mean fluorescence intensity (MFI) using ImageJ in four identical regions (non-overlapped images at 20× magnification) captured by fluorescence microscopy (n = 5–6 per group). For counting immunolabeled cells, the number of cells per defined tissue area was counted at 40× and 20× magnifications. Plaque-associated cells (microglia and $Ly6C^+$ monocytes) included cells at distances < 30 μm from the center of the amyloid plaque. Plaque-free cells included cells at distances > 30 μm from the center of the amyloid plaque. For counting the number of cells around plaques, microglia were selected based on DAPI-labeled nuclei. The result was presented as the total number of immunolabeled cells around plaques.

## 7. Enzyme-linked immunosorbent assay (ELISA) for Aβ1–42 quantification

The Amyloid β (1–42) Assay Kit (#27711, IBL, Tokyo, Japan) was used to measure amounts of Aβ42 (n = 7 per group). The test sample included 100 μL brain lysate, and all procedures for the assay were performed according to the manufacturer's guidance. Reagents were prepared at RT approximately 30 min before use.

## 8. Multiplex cytokine immunoassay

Expression levels of IL-1β, TNF-α, IFN-γ, and IL-4 in 5XFAD mouse brains were examined using a multiplex immunoassay (Bio-Plex mouse cytokine assay kit, Bio-Rad Laboratories, Hercules, CA, USA) (n = 5–6 per group). Brain tissues were lysed using the MicroRotofor™ Cell Lysis Kit (Bio-Rad Laboratories), and proteins in the homogenate were quantified using the bicinchoninic acid (BCA) assay kit (Pierce Biotechnology, Inc., Rockford, IL, USA). The assay was performed according to the manufacturer's instructions, and results were analyzed using the Bio-Plex Manager Software and Bio-Plex Data Pro™ software.

## 9. Real-time quantitative reverse transcription-PCR

Total RNA from brain tissue was isolated using the HiGene Total RNA Prep Kit (BIOFACT, Daejeon, Korea) according to the manufacturer's protocol and reverse-transcribed using the RT-PCR premix kit (Elpis Biotech Inc., Daejeon, Korea). Quantitative real-time PCR was performed using CFX96 (Bio-Rad) and SYBR green (Enzynomics™, Daejeon, Korea) (n = 4–5 per group). Primer sequences used for real-time PCR are presented in the table (Table 1).

## 10. Microarray

Total brain tissue RNA was extracted and pooled for microarray analysis (n = 3), performed using the Illumina MouseRef-8 v2 Expression BeadChip array (Illumina, Inc., San Diego, CA, USA) by Macrogen Inc. (Seoul, Korea). Export processing and analysis of arrayed data were performed using Illumina GenomeStudio v2011.1

(Gene Expression Module v1.9.0), and data were analyzed with the R v. 2.15.1 statistical software. Hierarchical cluster analysis was performed using the Permute Matrix. Heat maps were created using the Excel Spreadsheet software (Microsoft Corporation, Redmond, WA, USA) with conditional formatting. Gene expression rates in the AD and AD + Toxo groups were compared with those in the wild-type (WT) group. Positive correlations are depicted in yellow (increased expression) and negative (decreased expression) in blue. The color scale of the heat map represents the relative minimum (−3) and maximum (+3) values of each gene.

## 11. TUNEL staining for plaque-associated apoptotic microglia

TUNEL staining was performed on paraffin-embedded sections using the Cell Meter™ Fixed Cell and Tissue TUNEL Apoptosis Assay Kit (AAT Bio., Sunnyvale, CA, USA) according to the manufacturer's protocol. Briefly, sections were deparaffinized, rehydrated, and immersed in 4% paraformaldehyde for 20 min at RT. Then, sections were incubated in 20 μg/mL proteinase K for 10 min and fixed with 4% paraformaldehyde for 20 min. Subsequently, sections were incubated with 25 μL TUNEL reaction mixture for 60 min and immunostained with Iba1 Ab (Abcam) as the primary Ab and anti-goat Alexa Fluor 647 (Invitrogen, Carlsbad, CA, USA) as the secondary Ab. Finally, DAPI-stained sections were mounted. TUNEL positive (apoptotic) cells were observed using fluorescence microscopy at 40× magnification (n = 6 per group).

## 12. Statistics

All statistical analyses were performed using the GraphPad Prism 5 software (GraphPad, La Jolla, CA, USA). Data are presented as the mean ± standard error of the mean. For MFI fold change data in Figure 1.5–1.8, a one-way analysis of variance (ANOVA) followed by Dunnett's multiple comparisons test was used for statistical evaluation. To compare experimental groups, namely WT, AD, and AD + Toxo, one-way ANOVA followed by Tukey's multiple-comparison test was performed. Significant differences for the two groups were assessed using Student's t-test with Welch's correction. An asterisk (*) indicates a significant difference compared with the control ($p < 0.05$), and a sharp (#) indicates a significant difference among experimental groups ($p < 0.05$).

# RESULTS

## Study I: Changes in the proliferation of microglia induced by chronically infected *Toxoplasma gondii*

### *T. gondii* chronic infection-induced microglial proliferation in mouse brains

H&E-stained *T. gondii* cysts were detected during the 36-week infection period, indicating persistent infection (Figure 1.1). Simultaneously, the number of Iba1-stained microglia was increased from 3 weeks post-infection (PI) and maintained during the 36-week infection period (Figure 1.2). To investigate the proliferation of homeostatic microglia, the TMEM119 antibody was used for staining resident homeostatic microglia with the immunofluorescence assay (IFA) (Figure 1.3). The number of TMEM119-stained resident homeostatic microglia was also increased from 3 weeks PI and was maintained during the 36-week infection period (Figure 1.3). Activated microglia were co-stained with CD11b and Iba1 antibodies (Figure 1.4). The staining result for Iba1 and CD11b co-stained cells showed no significant increase during the 36-week infection period

### Quantification of immunofluorescence staining of microglia

The MFI calculated from the IFA image stained with Iba1 using ImageJ showed an increase in the hippocampus and cortex during the 36-week infection period, significantly increasing at 3 and 6 weeks PI ($p < 0.05$, Figure 1.5). By contrast, for TMEM119, the MFI exhibited a significant increase at 3, 6, and 36 weeks PI ($p < 0.05$, Figure 1.6) in the hippocampus and cortex during the 36-week infection period. Furthermore, the counting for Iba1 and CD11b co-stained cells showed no significant

increase during the 36-week infection period (Figure 1.7). Thus, most microglia proliferating after *T. gondii* infection were homeostatic microglia. Because cell proliferation is a consequence of mitosis, the significant increase in DAPI/Iba1/Ki67-stained mitotic microglia indicates that *T. gondii* infection induced microglial proliferation (yellow arrowhead and Iba1/Ki67-co-stained cells/mm$^2$ brain tissue; $p < 0.05$, Figure 1.8).

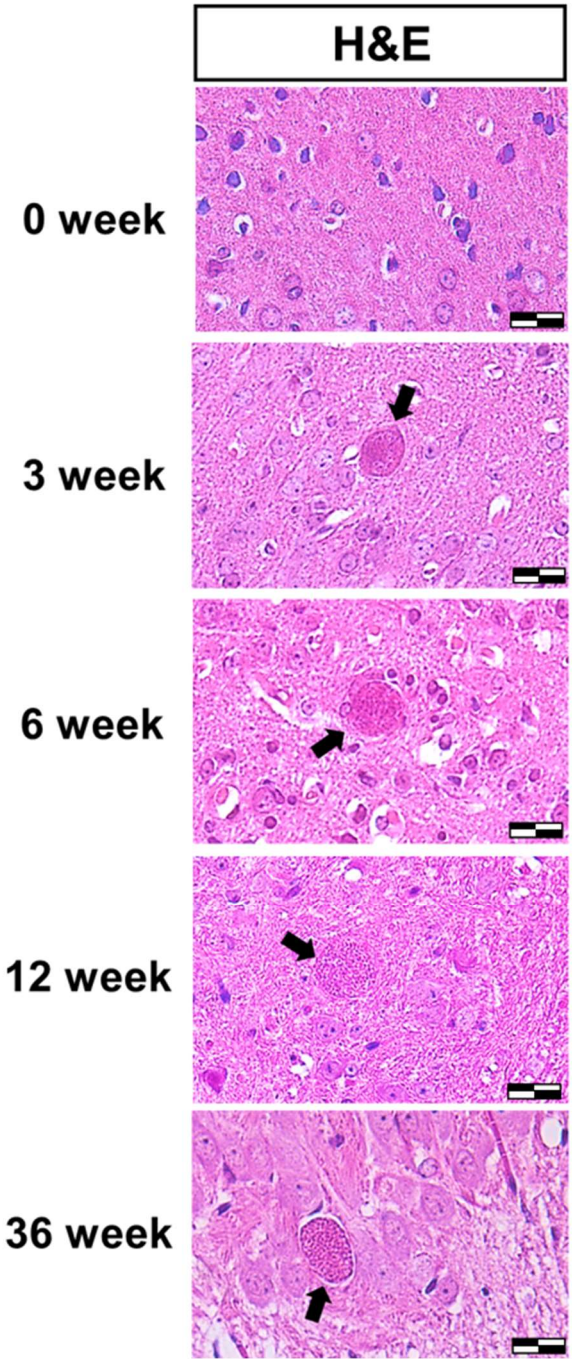


**Figure 1.1. Persistent infection of *T. gondii* during the 36 weeks**

*T. gondii* infection was confirmed by the presence of cysts in the brain tissue (H&E staining; scale bar: 20 μm). Black arrow indicates a *T. gondii* cyst in the brain parenchyma (H&E staining; scale bar: 20 μm).

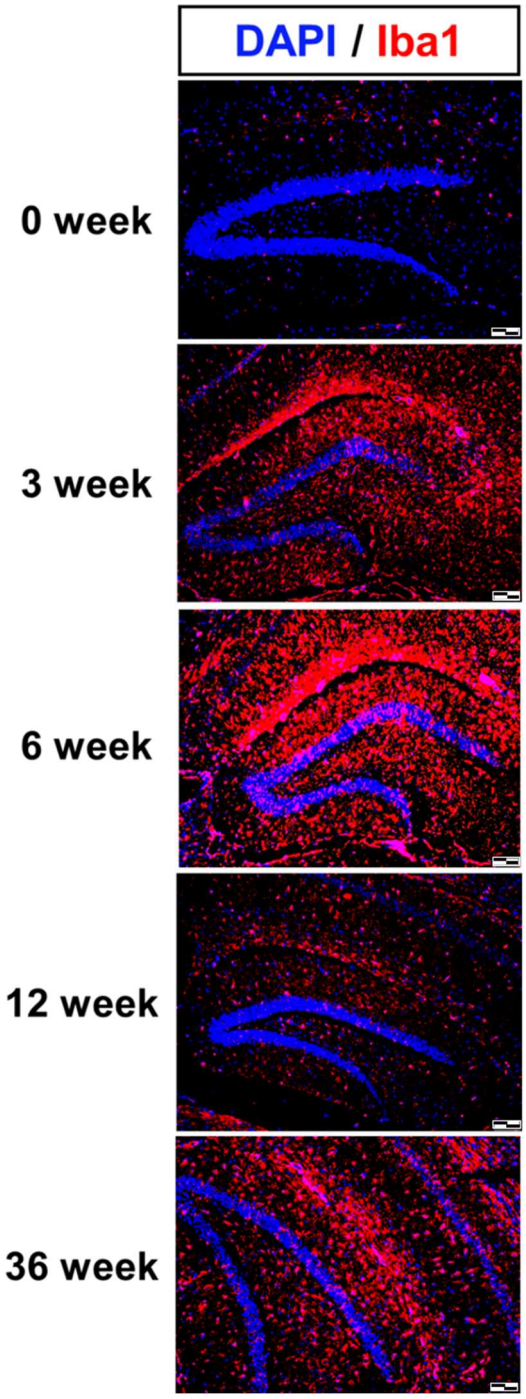


**Figure 1.2. Iba1-stained microglia was increased during *T. gondii* chronic infection**

Pan-microglia in the hippocampal formation were stained with Iba1 (red; scale bar: 100 μm).

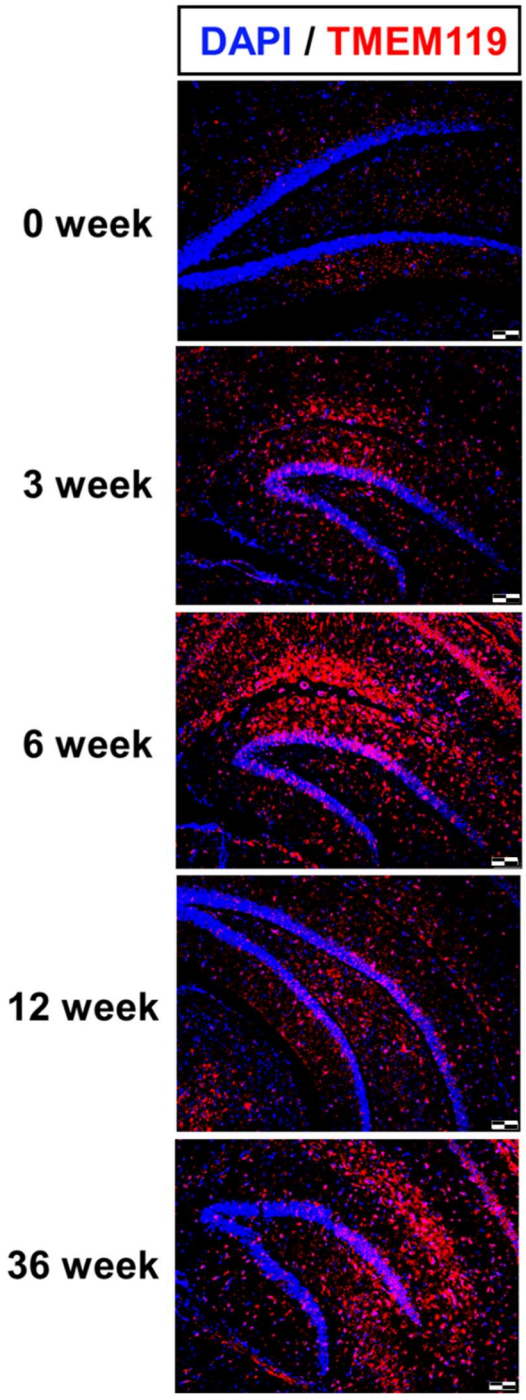


**Figure 1.3. TMEM119-stained homeostatic microglia was increased during *T. gondii* chronic infection**

Resident homeostatic microglia in the hippocampal formation were stained with TMEM119 (red; scale bar: 100 μm).

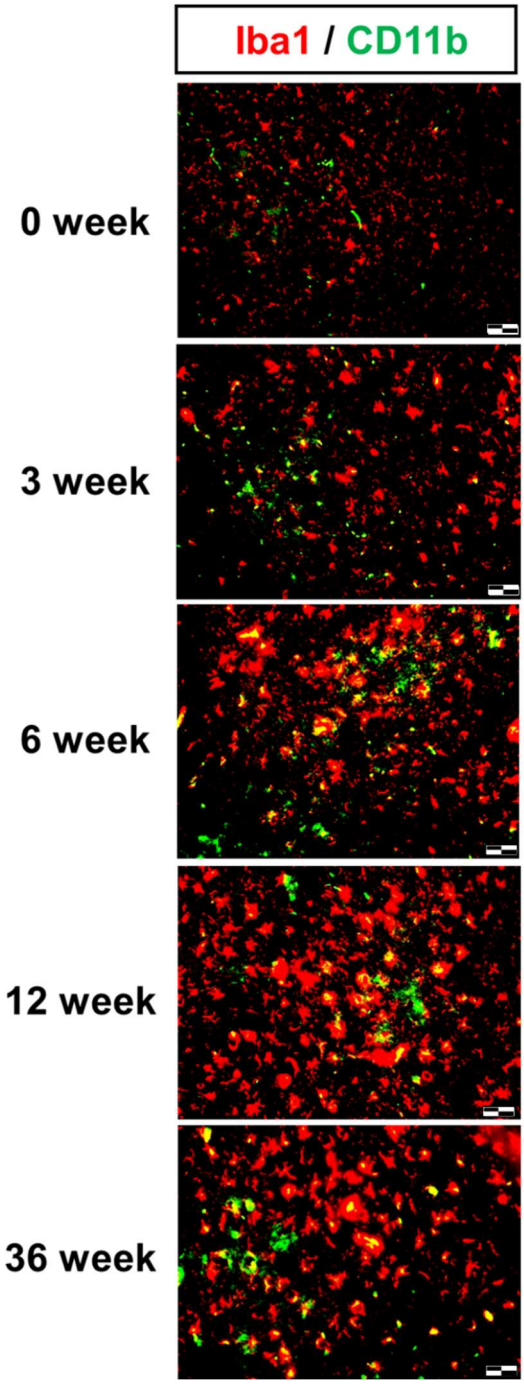


**Figure 1.4. Staining results of Iba1 and CD11b co-positive activated microglia during *T. gondii* chronic infection**

Activated microglia were co-stained with CD11b and Iba1 (green and red, respectively; scale bar: 50 μm).

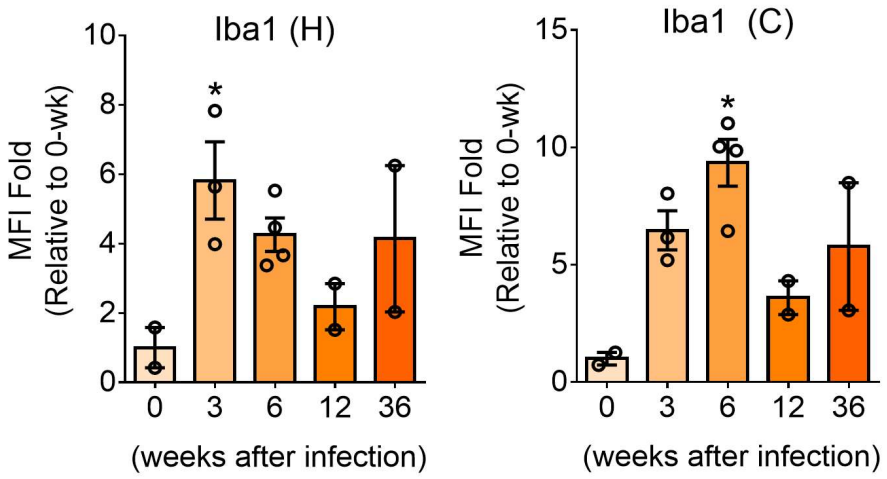


**Figure 1.5. MFI calculated from the IFA image stained with Iba1 in *T. gondii* chronic infection mouse model**

The MFI was calculated from Iba1-stained microglia using ImageJ. The fold changes of the MFI at 3, 6, 12, and 36 weeks after infection were compared with those of the control (0 weeks). To quantify the area covered by microglia in the cortex and hippocampus, slides stained with Iba1 Ab were used for calculating MFI using ImageJ in four identical regions (non-overlapped images at 20× magnification) captured by fluorescence microscopy (n = 2–4 per group). Quantification of MFI intensity; two brain sections per mouse. Data are presented as mean ± SEM. *Statistical significance compared with the control (*$p < 0.05$). H, hippocampus; C, cortex.

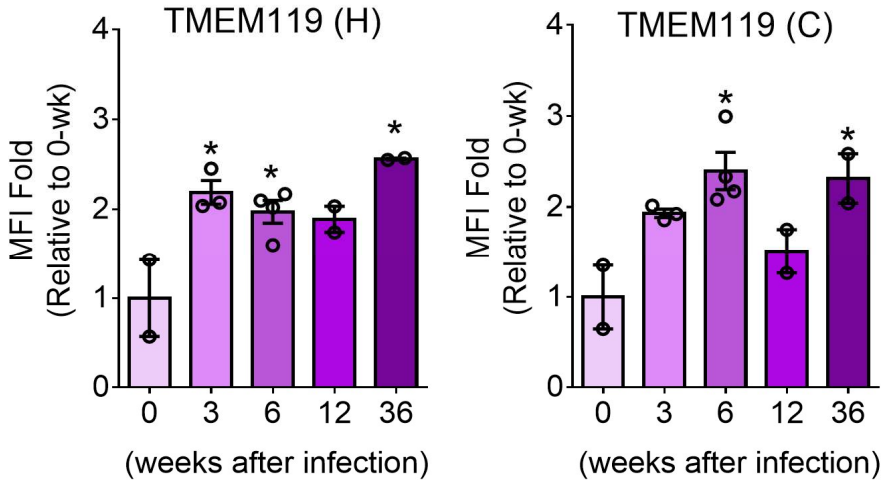


**Figure 1.6. MFI calculated from the IFA image stained with TMEM119 in *T. gondii* chronic infection mouse model**

The MFI was calculated from TMEM119-stained homeostatic microglia using ImageJ. The fold changes of the MFI at 3, 6, 12, and 36 weeks after infection were compared with those of the control (0 weeks). To quantify the area covered by microglia in the cortex and hippocampus, slides stained with TMEM119 Ab were used for calculating MFI using ImageJ in four identical regions (non-overlapped images at 20× magnification) captured by fluorescence microscopy (n = 2–4 per group). Quantification of MFI intensity; two brain sections per mouse. Data are represented as the mean ± SEM. *Statistical significance compared with the control (* $p < 0.05$). H, hippocampus; C, cortex.

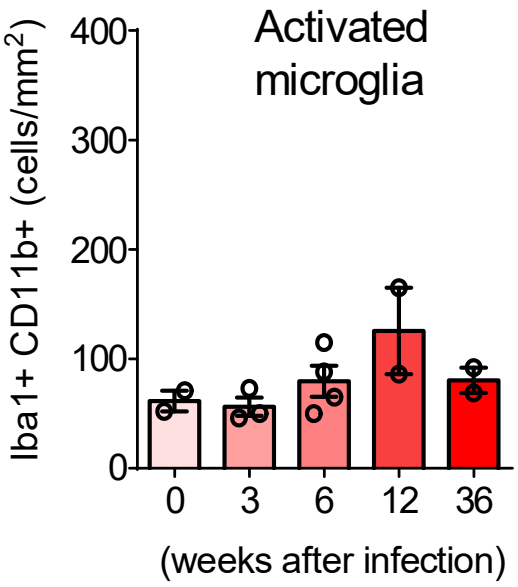


**Figure 1.7. Counting results of Iba1 and CD11b co-stained activated microglia in *T. gondii* chronic infection mouse model**

The number of activated microglia (Iba1+/CD11b+) was designated by cell number per $mm^2$ of the brain tissue. Counting results of activated microglia at 3, 6, 12, and 36 weeks after infection were compared with those of the control (0 weeks). The number of Iba1 and CD11b co-positive cells per defined tissue area ($1mm^2$) was counted at 20× (n = 2–4 per group). Quantification of cell counting; two brain sections per mouse. Data are presented as mean ± SEM.

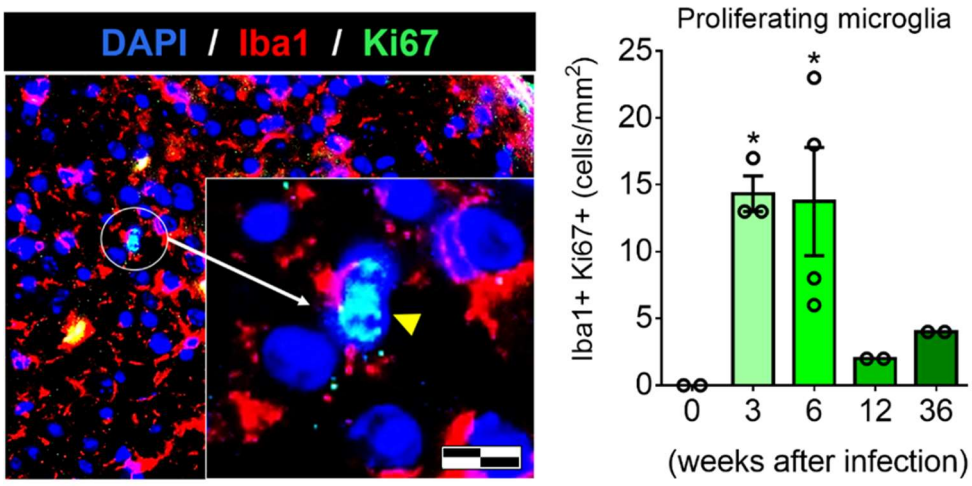


**Figure 1.8. Ki67-positive proliferative microglia during chronic *T. gondii* infection**

Proliferating microglia were stained with Ki67 and Iba1. The yellow arrowhead shows microglial cells in the mitotic phase (sky blue) co-stained with DAPI (blue) and Ki67 (green), and the number of proliferating microglia (Iba1+/Ki67+) was designated by cell number/$mm^2$ brain tissue. Scale bar: 20 μm. The number of Iba1 and Ki67 co-positive cells per defined tissue area (1$mm^2$) was counted at 40× (n = 2–4 per group). Quantification of cell counting; two brain sections per mouse. Data are presented as mean ± SEM. *Statistical significance compared with the control (* $p < 0.05$).

**Relative expression of microglia proliferation markers and phenotype markers for *T. gondii*-infected mouse brains during chronic infection**

To investigate genetic changes that induce microglial proliferation, microarray analysis was performed for genes encoding microglial trophic factors (*Il1β*, *Tnfα*, *Mcsf*, and *NFKB1*), microglia markers (*Iba1*), resident homeostatic microglial markers (*P2ry13*, *Cx3cr1*, and *Tmem119*), and polarization markers (*Ifnγ*, *Il4*, *Cd86*, and *Cd206*) at 3, 6, 12, and 36 weeks PI (Figure 1.9). Genes encoding microglial trophic factors and resident homeostatic markers were continuously increased, except for the decrease in *Mcsf* at 36 weeks, during chronic *T. gondii* infection (Figure 1.9). At this time, the direction of microglial polarization was not M2 (*Il4* and *Cd206*) but M1 (*Ifnγ* and *Cd86*). These findings revealed that chronic *T. gondii* infection in the brain induced M1-type activation of microglia through the continuous proliferation of homeostatic microglia. Importantly, homeostatic microglial proliferation was maintained during chronic *T. gondii* infection.

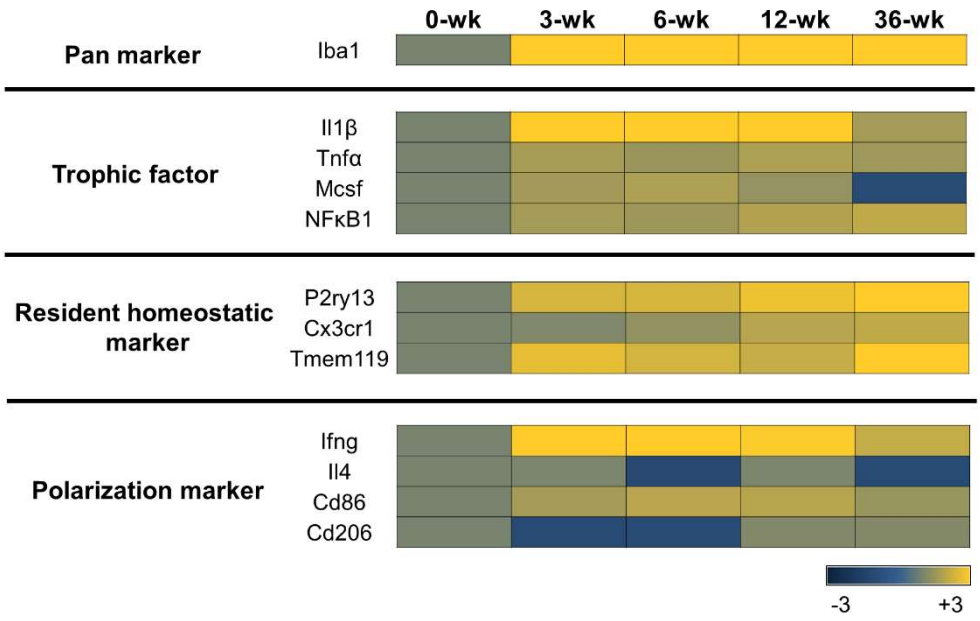


**Figure 1.9. Microarray analysis of genes encoding trophic factors, homeostatic markers, and M1 and M2 markers in *T. gondii*-infected mouse brains**

Transcript levels of trophic factors and microglia phenotype markers were measured in *Toxoplasma gondii*-infected mouse brains using microarray analysis. Each column represents infection periods from 0 to 36 weeks post-infection. The color scale corresponds to the relative expression of the markers for the minimum (−3) and maximum (+3) of all values.

## Study II: Effects of *Toxoplasma gondii* infection on amyloid plaque burden in 5XFAD Alzheimer's disease mouse model

### Amyloid-β plaque reduction in *T. gondii*-infected 5XFAD mouse brains

5XFAD mice were used to investigate microglial proliferation and activation after *T. gondii* infection. *T. gondii* cysts (black arrows in H&E and Congo red staining) were found around Aβ plaques (blue arrowhead in Congo red staining) in the brain tissue at 40 weeks PI (Figure 2.1). *T. gondii*-infected (AD + Toxo group) 5XFAD mice exhibited a reduction in the Aβ plaque burden in the hippocampus and cortex compared with non-infected mice (AD group) (Figure 2.2). Moreover, the number of acidophilic neurons, which indicate a neuropathological state in layer V of the cortex, decreased in the AD + Toxo group compared with the AD group. (Figure 2.2). The number of dense-core plaques stained with Congo red dye was significantly decreased in the hippocampi and cortexes of the AD + Toxo group compared with the AD group ($p < 0.05$, Figure 2.3). Evaluating the amount of Aβ1–42 in brain tissue lysate using the amyloid β1–42 ELISA kit revealed that the amount of Aβ1–42 was significantly reduced in the AD + Toxo group (67.27 ± 18.73 pg/mL) compared with the AD group (127.5 ± 6.651 pg/mL) ($p < 0.05$, Figure 2.4).

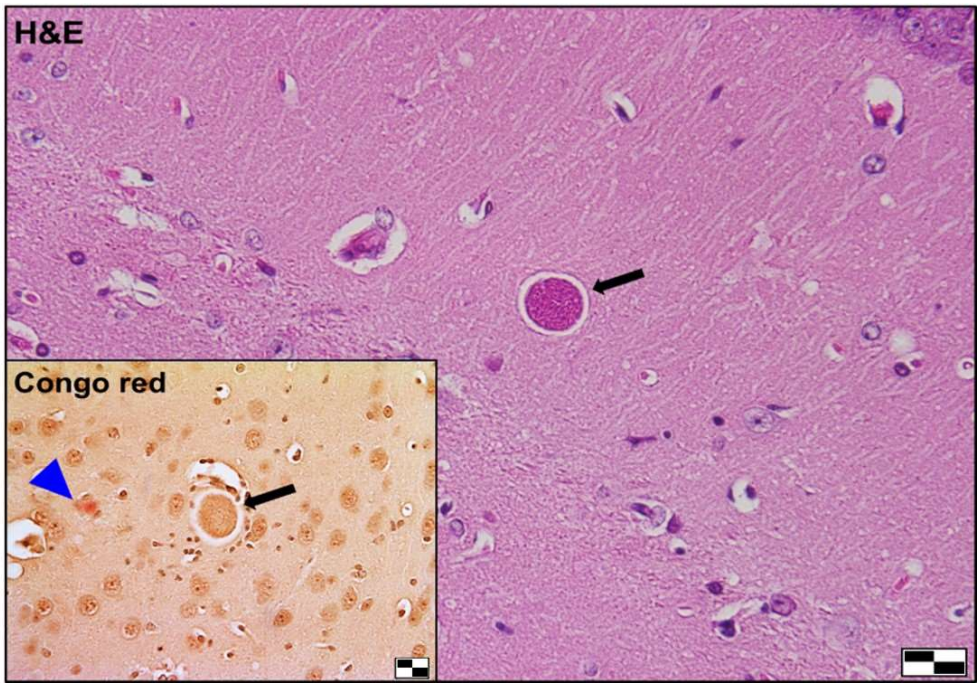


**Figure 2.1. 5XFAD mice were chronically infected with *T. gondii* strain ME49**

A *T. gondii* cyst (black arrow) and stained amyloid plaque (blue arrowhead) in a brain section (H&E and Congo red staining) at 40 weeks post- *T. gondii* infection. Scale bar: 20 µm.

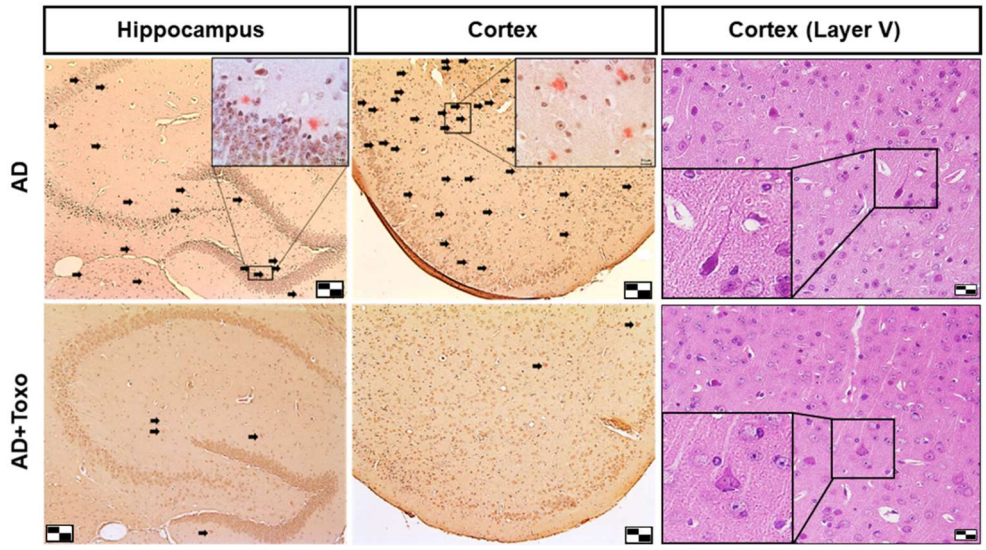


**Figure 2.2. Amelioration of amyloid plaque deposition and neurodegeneration induced by chronic *T. gondii* infection in a 5XFAD mouse**

Dense core plaques (black spots) were stained using Congo red dye (scale bar: 100 μm) and acidophilic neurons (black box) in cortical layer V (scale bar: 20 μm).

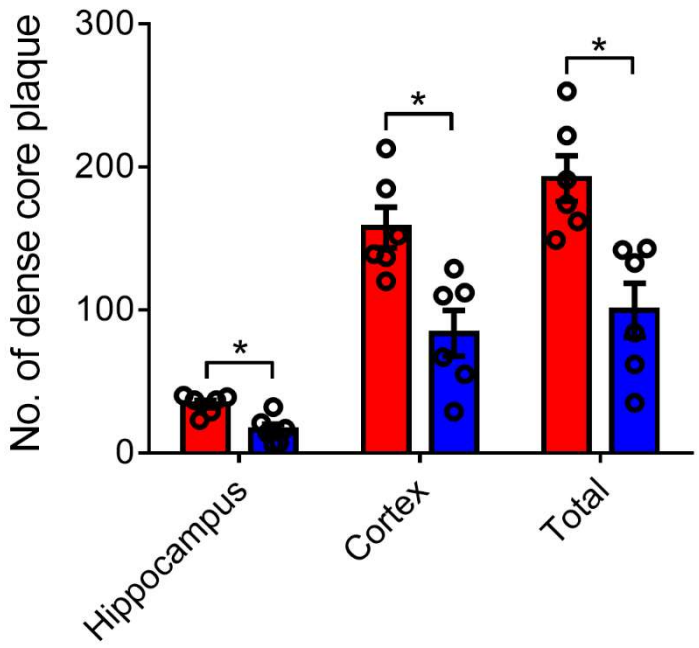


**Figure 2.3. Number of dense-core plaques counted in Congo red-stained mouse brains**

The number of dense-core plaques stained with Congo red dye was significantly decreased in the *T. gondii* infected 5XFAD mice (n = 6 per group). Data are presented as mean ± SEM. *Statistical significance compared with the control (* $p < 0.05$).

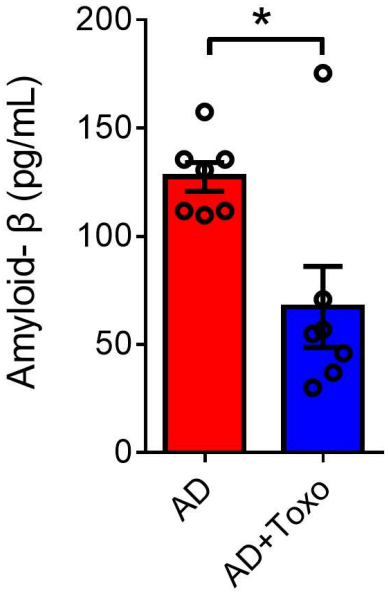


**Figure 2.4. The concentration of Aβ in brain tissue lysate analyzed by ELISA**

The amount of Aβ1–42 in brain tissue lysate was measured using the amyloid β1–42 ELISA assay kit (n = 7 per group). Data are presented as mean ± SEM. *Statistical significance compared with the control (* $p < 0.05$).

**Microglial proliferation in *T. gondii*-infected 5XFAD mouse brain**

Considering the importance of microglia in clearing Aβ plaques, this study analyzed microglial accumulation around Aβ plaques (Figure 2.5). Microglial cells (DAB-stained, dark brown) were accumulated around amyloid plaques in both AD and AD + Toxo groups; however, the number of microglia around the Aβ plaque was higher in the AD + Toxo group than in the AD group (Figure 2.5). Additionally, more microglia selectively were adhered to plaques than *T. gondii* tissue cysts (Figure 2.6). To compare the degree of microglial proliferation in the AD and AD + Toxo groups, the hippocampi and cortexes were stained using Iba-1 Ab (red). The degree of microglial proliferation was greater in the AD + Toxo group than in the AD group (Figure 2.7). To evaluate this difference numerically, when the MFI of Iba-1 staining in the AD group was defined as numerically one-fold, the fold change of the MFI in the AD + Toxo group was significantly increased in both the hippocampus and cortex ($p < 0.05$, Figure 2.7). Similarly, resident homeostatic microglial cells stained with the TMEM119 Ab were significantly increased in the AD + Toxo group, in both the hippocampus and cortex, compared with the AD group ($p < 0.05$, Figure 2.8).

**Relative expression of microglia proliferation markers and phenotype markers for *T. gondii* infected 5XFAD mouse brains compared with 5XFAD mouse brains**

To investigate the molecular signals that induce homeostatic microglial proliferation in the AD + Toxo group, microglial trophic factors (IL-1β and TNF-α) and inducers (IFN-γ and IL-4) for the polarization of M1 and M2 microglia were examined using

ELISA and microarray analysis (Figure 2.9, 2.10). Data revealed that the proliferation of homeostatic microglia in the AD + Toxo group correlated with a significant increase in IL-1β and TNF-α levels and the expression of trophic factors (*Il1β*, *Tnfα*, *Mcsf*, and *NFKB1*) ($p < 0.05$, Figure 2.9, 2.10). Thus, the polarization of proliferated microglia can be inferred from the expression of M1- and M2-inducing cytokines (IFN-γ and IL-4). Moreover, the expression of M1-inducing factors (IFN-γ at the protein level and *Ifnγ* and *Cd86* at the gene level) was greater than that for M2-inducing factors (IL-4 at the protein level and *Il4* and *Cd206* at the gene level) when comparing the AD + Toxo group with the AD group ($p < 0.05$, Figure 2.9, 2.10). Homeostatic microglia markers, namely *P2ry13*, *Cx3cr1*, and *Tmem119*, were found to increase in the AD + Toxo group compared with the AD group (Figure 2.10). Thus, the *T. gondii*-mediated increase in microglial proliferation and polarization may be beneficial for reducing the Aβ plaque burden.

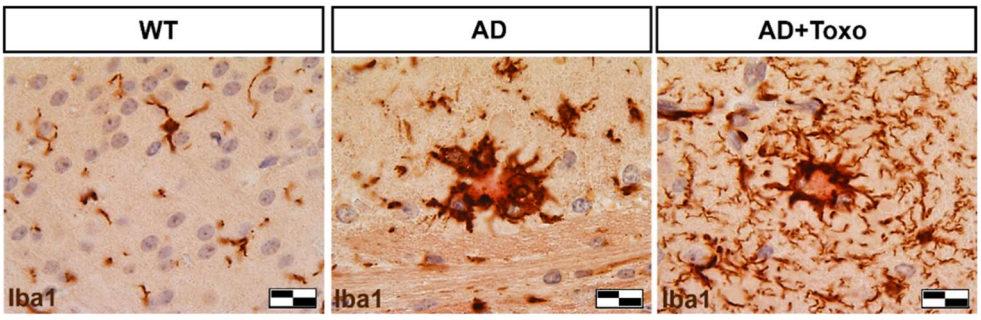


**Figure 2.5. DAB-color immunohistochemistry of microglia around Aβ plaques**

Gathered microglia and amyloid plaques were stained with Iba1 and Congo red (brown and red, respectively; scale bar: 20 μm).

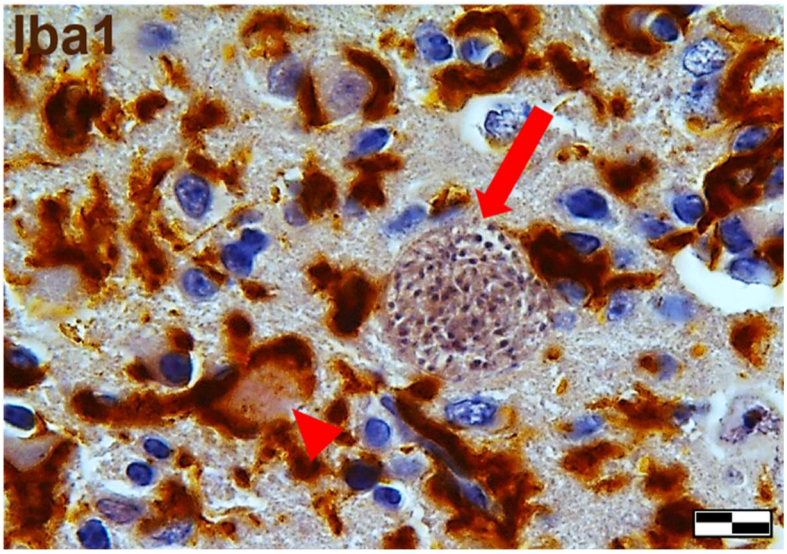


**Figure 2.6. Microglia gathered around amyloid plaque in a 5XFAD mouse chronically infected with *T. gondii***

A *T. gondii* tissue cyst (red arrow) and Congo red-stained amyloid plaque (red arrowhead) with DAB-stained microglia (brown) in a brain section at 40 weeks post-infection. Scale bar: 10 μm.

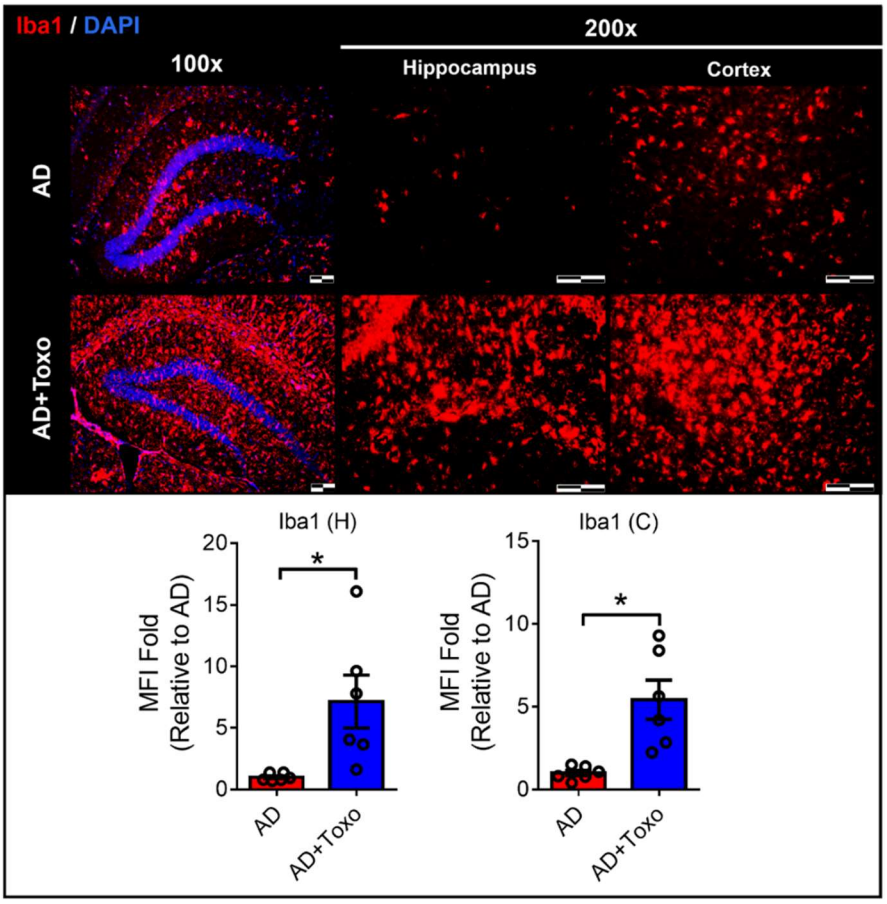


**Figure 2.7. MFI calculated from the IFA image stained with Iba1 in a 5XFAD mouse**

MFI was calculated from Iba1-stained microglia using ImageJ. The fold changes of MFI in the *T. gondii*-infected AD group (AD + Toxo) were compared with those of the control group (AD). To quantify the area covered by microglia in the cortex and hippocampus, slides stained with Iba1 Ab were used for calculating MFI using ImageJ in four identical regions (non-overlapped images at 20× magnification) captured by fluorescence microscopy (n = 6 per group). Data are presented as mean ± SEM. *Statistical significance compared with the control (* $p < 0.05$). H, hippocampus; C, cortex. Scale bar: 100 μm.

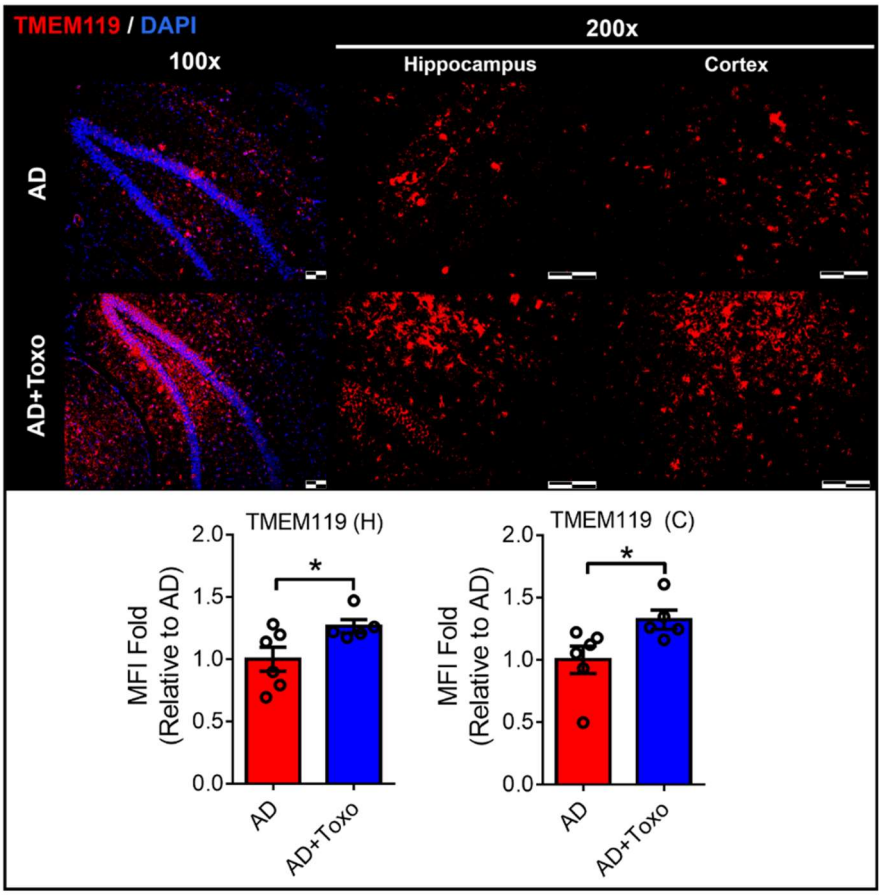


**Figure 2.8. MFI calculated from the IFA image stained with TMEM119 in a 5XFAD mouse**

The MFI was calculated from TMEM119-stained homeostatic microglia using ImageJ. The fold changes of the MFI in the *T. gondii*-infected AD group (AD+Toxo) were compared with those of the control (AD). To quantify the area covered by microglia in the cortex and hippocampus, slides stained with TMEM119 Ab were used for calculating MFI using ImageJ in four identical regions (non-overlapped images at 20× magnification) captured by fluorescence microscopy (n = 5-6 per group). Data are presented as mean ± SEM. *Statistical significance compared with the control (* $p < 0.05$). H, hippocampus; C, cortex. Scale bar: 100 μm.

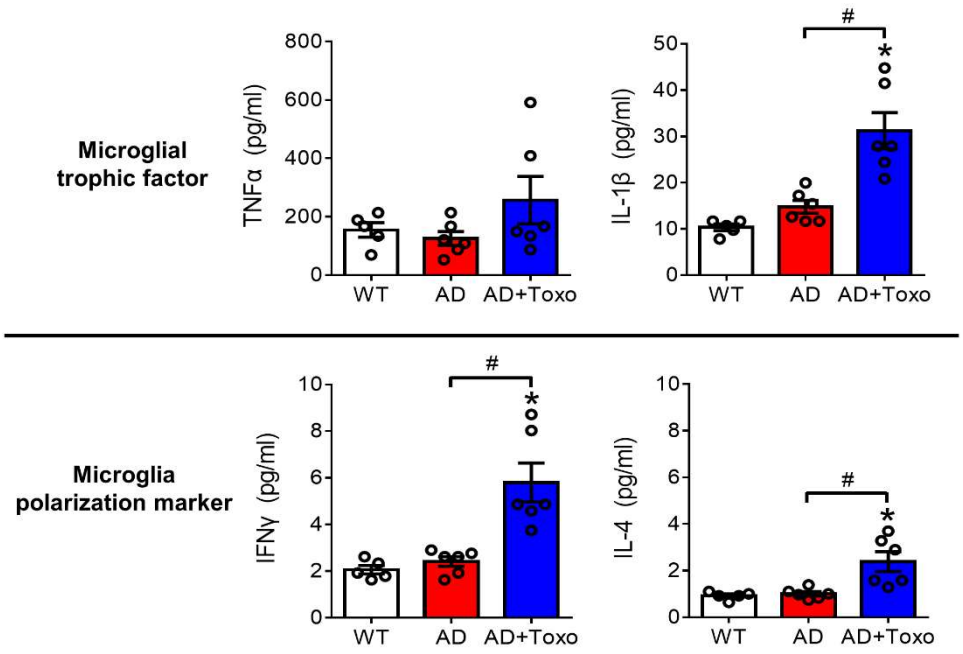


**Figure 2.9. Protein expression of microglial trophic factors (IL-1β and TNF-α) and microglial polarization inducers (IFN-γ and IL-4) in 5XFAD mouse brain lysate**

Microglial trophic factors (IL-1β and TNF-α) and polarization inducers (IFN-γ and IL-4) of M1 and M2 microglia were examined using ELISA assay (n = 5-6 per group). Data are presented as the mean ± SEM. * Statistical significance compared with the control (* $p < 0.05$). # Statistical significance compared with each experimental group (# $p < 0.05$).

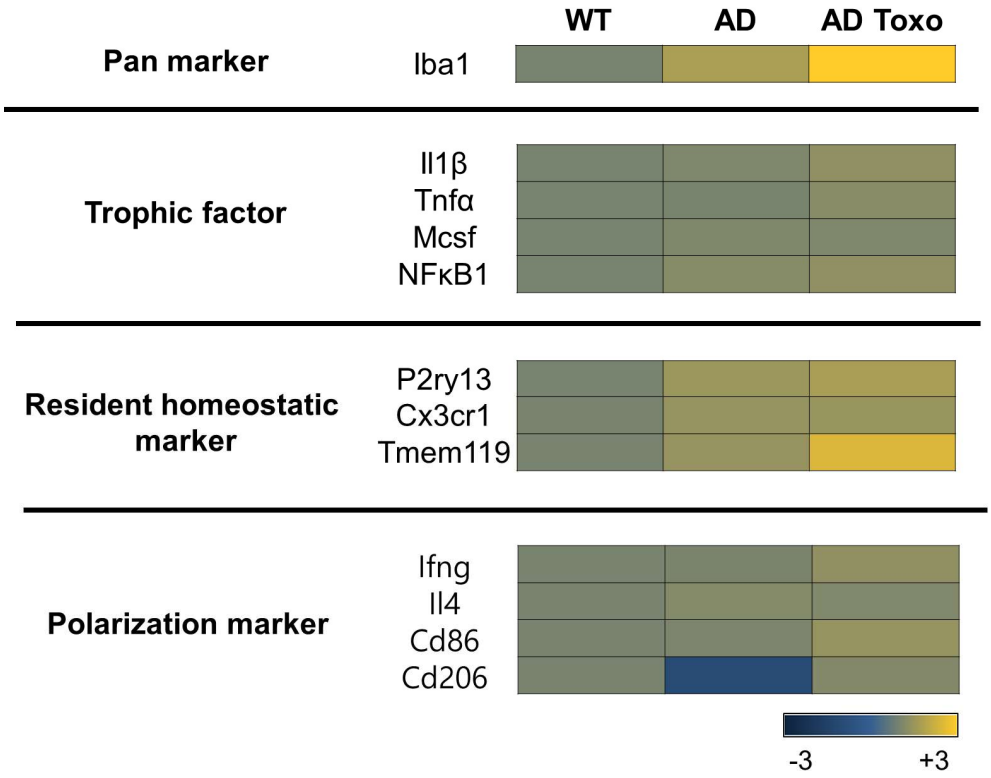


**Figure 2.10. Microarray analysis of genes encoding trophic factors, homeostatic markers, and M1 and M2 markers in 5XFAD mouse brains**

Transcript levels of trophic factors and microglia phenotype markers were measured in 5XFAD mouse brains using microarray analysis. Relative expressions in the AD and AD + Toxo groups were compared with the gene expression in WT mice. The color scale corresponds to the relative expression of the markers for the minimum (−3) and maximum (+3) of all values.

**Microglial proliferation in *T. gondii*-infected 5XFAD mouse brains**

To investigate the plaque-associated pattern of microglia responsible for plaque clearance, the distribution of plaque-associated microglia and plaque-free microglia was evaluated by co-staining with methoxy-XO4 (a fluorescent probe for detecting plaques) and Iba1 Ab (Figure 2.11). Microglia in close contact with an amyloid plaque, such as within a 30-μm radius, were termed plaque-associated microglia, and those outside a 30-μm radius were termed plaque-free microglia (Figure 2.11). The morphology of the dense core amyloid plaque stained with methoxy-XO4 is large and unspecified (displayed as a white mass), and the number of microglia (red fluorescence) in close contact with the amyloid plaque border was higher in the AD + Toxo group than in the AD group (Figure 2.11). To compare the number of plaque-associated or plaque-free microglia, we collected 60 amyloid plaques from the brain (10 randomly selected plaques per mouse × 6 mice per group) and counted microglia around the plaques (Figure 2.11). The numbers of both plaque-associated and plaque-free microglia were significantly increased in the AD + Toxo group compared with the AD group, indicating the migration of newly proliferated homeostatic microglia from the far side (plaque-free pattern) to the near side of the plaque (plaque-associated pattern) ($p < 0.05$, Figure 2.11). To confirm this, the resident homeostatic microglia surrounding the amyloid plaques were analyzed by co-staining with Iba1 (red), TMEM119 (green), and methoxy-XO4 (blue). Few TMEM119-stained microglia was surrounded amyloid plaques in the AD group, whereas several TMEM119-expressing microglia (yellow) were seen in the AD + Toxo group (Figure 2.12). When counting the number of TMEM119-expressing microglia around

amyloid plaques, the number of plaque-associated homeostatic microglia was significantly increased in the AD + Toxo group compared with the AD group ($p < 0.05$, Figure 2.12). Moreover, because *T. gondii* infection can recruit $Ly6C^+$ monocytes, which inhibit amyloidosis, the accumulation of $Ly6C^+$ monocytes around amyloid plaques was evaluated (Figure 2.13). Few $Ly6C^+$ cells (green) were accumulated around amyloid plaques in both the AD- and AD + Toxo groups; accordingly, the number of plaque-associated $Ly6C^+$ cells exhibited no difference between AD- and AD + Toxo groups (Figure 2.13). Thus, the ablation of amyloid plaques in the brain with AD progression may proceed through microglia but not through $Ly6C^+$ monocytes.

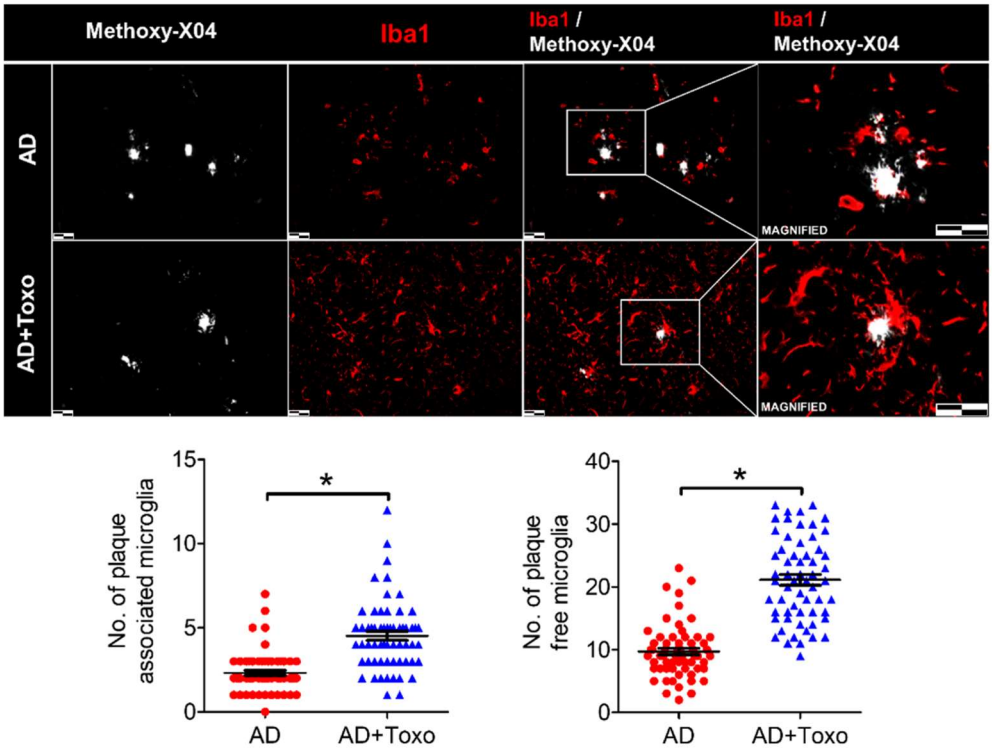


**Figure 2.11. Counting results of plaque-associated microglia and plaque-free microglia in a 5XFAD mouse**

Iba-1-stained microglia (red) around methoxy-XO4-stained amyloid β (Aβ) plaques (white). The counting result of microglia (plaque-associated or plaque-free) found around 60 amyloid plaques distributed in the brain (10 randomly selected plaques per mouse × 6 mice per group). Scale bar: 25 μm. Data are presented as mean ± SEM. *Statistical significance compared with the control (* $p < 0.05$).

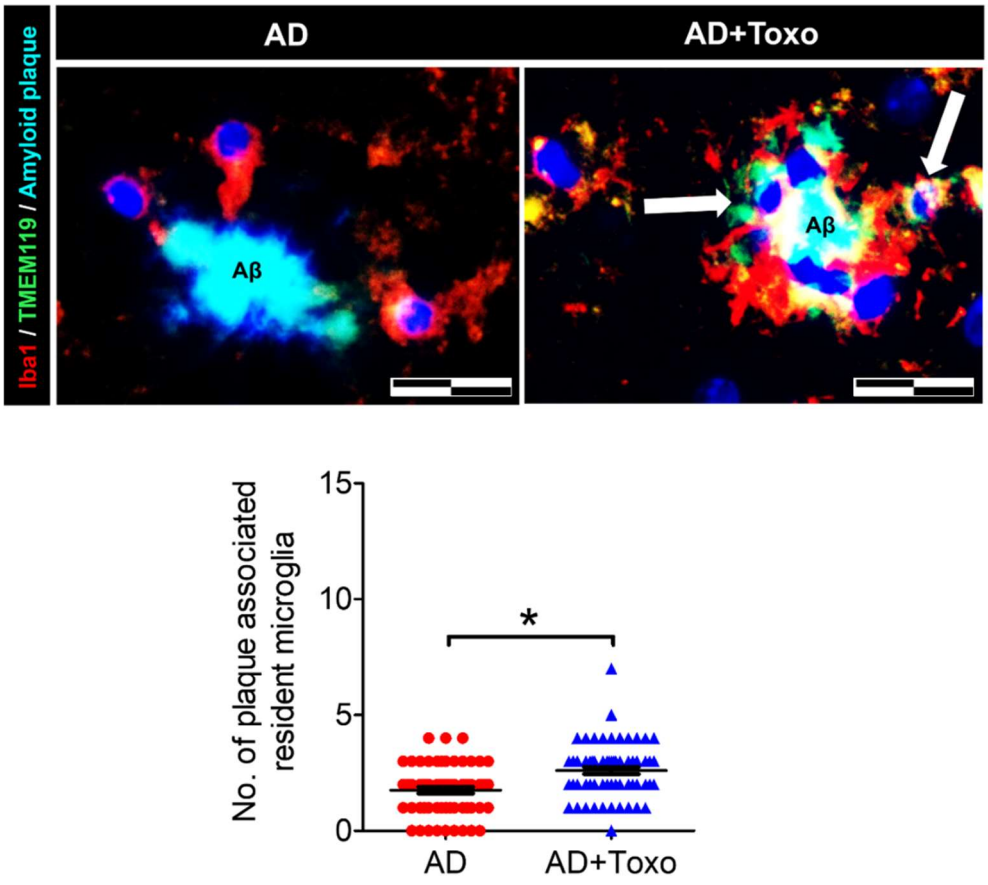


**Figure 2.12. Counting results of plaque-associated homeostatic microglia in a 5XFAD mouse**

Plaque-associated homeostatic microglia (yellow, due to co-staining of Iba-1 (red) and TMEM119 (green) and indicated by an arrow). The number of plaque-associated homeostatic microglial cells found around 60 amyloid plaques distributed in the brain (10 randomly selected plaques per mouse × 6 mice per group). Scale bar: 20 μm. Data are presented as mean ± SEM. *Statistical significance compared with the control (* $p < 0.05$).

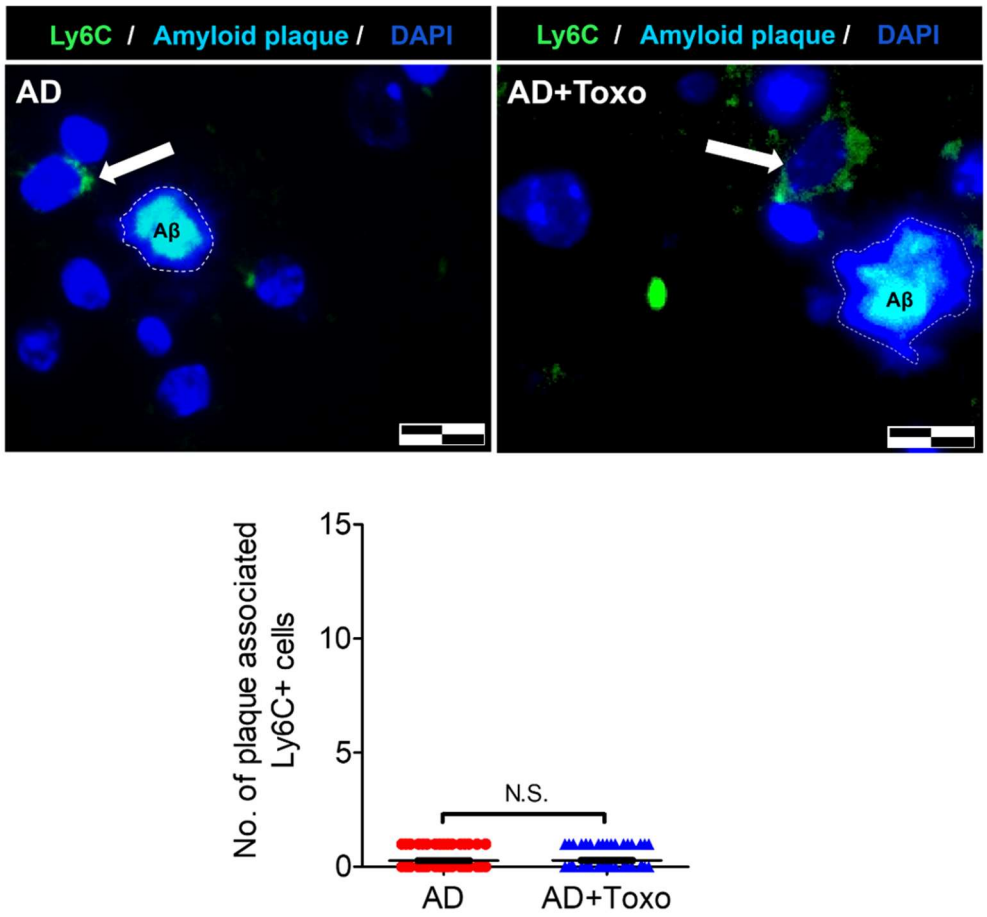


**Figure 2.13. Counting results of plaque-associated Ly6C$^{+}$ monocytes in a 5XFAD mouse**

Ly6C+ monocytes (green) accumulated around Aβ plaques in the brain tissues of both the AD and AD + Toxo groups. The white arrow indicates Ly6C+ (green) monocytes. The number of plaque-associated Ly6C+ monocytes found around 60 amyloid plaques distributed in the brain (10 randomly selected plaques per mouse × 6 mice per group). Scale bar: 20 μm. Data are presented as mean ± SEM. *Statistical significance compared with the control (* $p < 0.05$).

**Switching of homeostatic microglia to the DAM phenotype followed by microglial phagocytosis for plaque clearance**

In AD, homeostatic microglia are activated to clear plaques. As the presence of polarized DAM microglia is important for clearing amyloid plaques, the expression of DAM-related genes was investigated in the AD and AD + Toxo groups and compared with that of uninfected WT mice (Figure 2.14). Compared to the AD group, gene expression for the overall DAM phenotype, including *Apoe*, *Ax1*, *Clec7a*, *Cst7*, and *Trem2*, was reduced in the AD + Toxo group. By contrast, expression of the homeostatic microglia gene *Tmem119* was increased (Figure 2.14). Microarray gene expression and quantitative gene expression analysis of DAM (*Cst7*) and homeostatic (*Tmem119*) markers revealed that Cst7 was predominantly expressed in the AD group and TMEM119 in the AD + Toxo group ($p < 0.05$, Figure 2.14, 2.15). These results suggested that most microglia in the AD group were converted to the DAM phenotype. In contrast, in the AD + Toxo group, many homeostatic microglia were newly proliferated, although they were converted to the DAM phenotype. To visually check for switching to the DAM phenotype, microglia were co-stained with Alexa 568-conjugated Iba1 (red) and Alexa 488-conjugated TREM2 around the methoxy-XO4-labeled Aβ plaque (Figure 2.16). Co-labeling of Iba1 and TREM2 (shown in yellow) could be seen around the methoxy-XO4-labeled Aβ plaque; the number of co-labeled microglia surrounding this Aβ plaque was higher in the AD + Toxo group than in the AD group (Figure 2.16). Thus, newly proliferated homeostatic microglia in the AD + Toxo group were converted to the DAM phenotype and they were around the Aβ plaque. Moreover, another DAM-specific

microglia marker, namely lipoprotein lipase (LPL), was expressed in microglial cells around the Aβ plaque in both AD and AD + Toxo groups (green; Figure 2.17). Microglia co-stained with Alexa 488-conjugated LPL (green) and Alexa 568-conjugated Iba-1 (red) are shown in yellow; most plaque-associated microglia switched to the DAM phenotype in both the AD and AD + Toxo groups (Figure 2.17). However, considering that the sustained proliferation of homeostatic microglia appeared in the AD + Toxo group but not in the AD group, the pool of microglia capable of removing plaque was sufficient in the AD + Toxo group but not in the AD group. To define the role of the microglia recruited around the Aβ plaque, lysosomal degradation of the Aβ plaque was investigated by evaluating the colocalization of Iba1 (red) and lysosomal-associated membrane glycoprotein 1 (LAMP1; green) (Figure 2.18). Iba1 and LAMP1 colocalization is shown in yellow; lysosomal degradation and clearance of the Aβ plaque were indicated by the closed association between LAMP1 and the Aβ plaque. The Iba1-positive microglia associated with the Aβ plaque (white) expressing LAMP1 indicated lysosomal degradation, which could be seen as internalized puncta. In Figure 2.18, two amyloid β plaques, fragmented through lysosomal degradation within the microglia, were represented as “a” and “b.” Enlarged images (“a” and “b”) showed microglia with fragmented amyloid β plaques. Similar degree of lysosomal degradation of the Aβ plaque, indicated by internalized puncta (yellow arrow) per microglial cell, was observed in plaque-associated microglia of both AD + Toxo and AD groups (Figure 2.19).

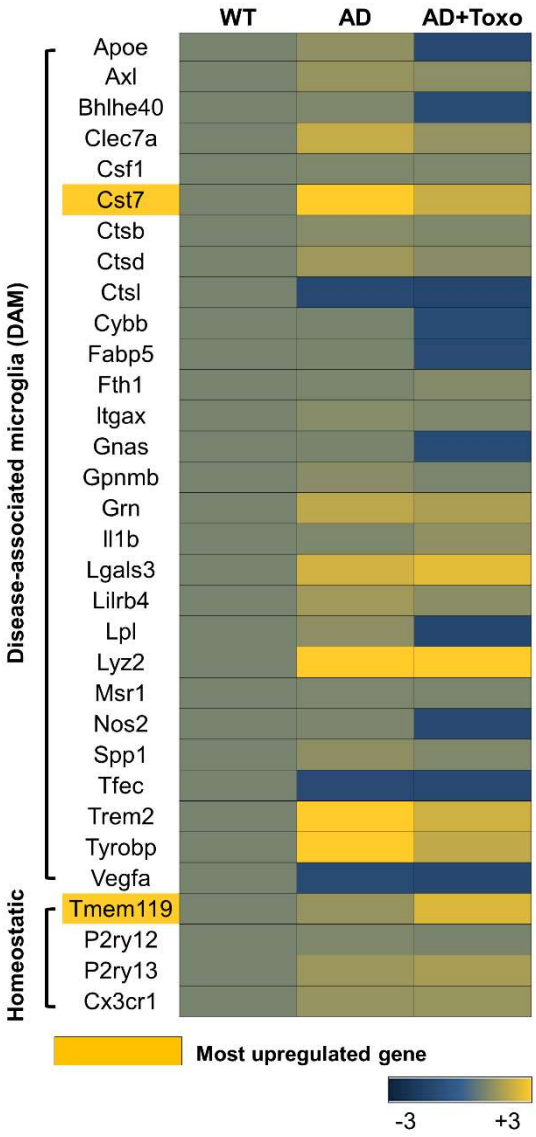


**Figure 2.14. Microarray analysis of genes encoding DAM or homeostatic microglial markers in 5XFAD mouse brains**

Transcript levels of DAM or homeostatic markers of microglia investigated by gene array analysis in 5XFAD mice. Relative expressions in the AD and AD + Toxo groups were compared with the gene expression in WT mice. The color scale corresponds to the relative expression of the markers for the minimum (−3) and maximum (+3) of all values.

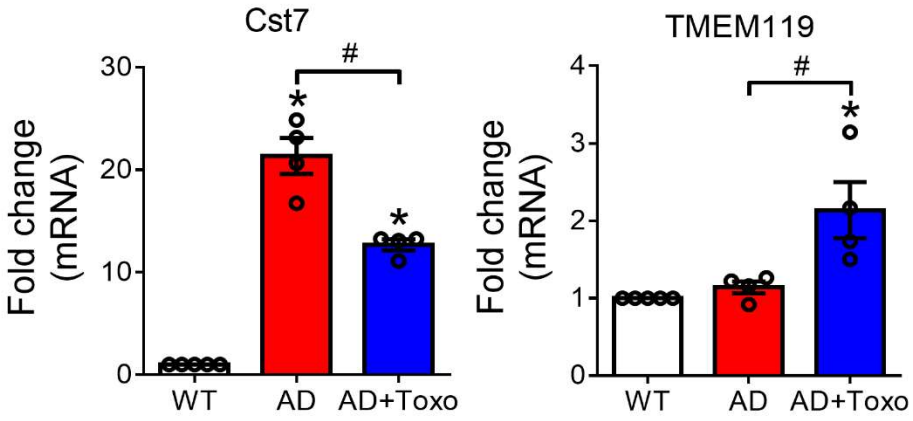


**Figure 2.15. Quantitative gene expression analysis of the most upregulated DAM marker (Cst7) and homeostatic marker (TMEM119) in 5XFAD mouse brains**

The most upregulated DAM (Cst7) and homeostatic markers (TMEM119) in the microarray analysis were examined using quantitative reverse transcription polymerase chain reaction analysis. Data are presented as mean ± SEM. * Statistical significance compared with the control (* $p < 0.05$). # Statistical significance compared with each experimental group (# $p < 0.05$).

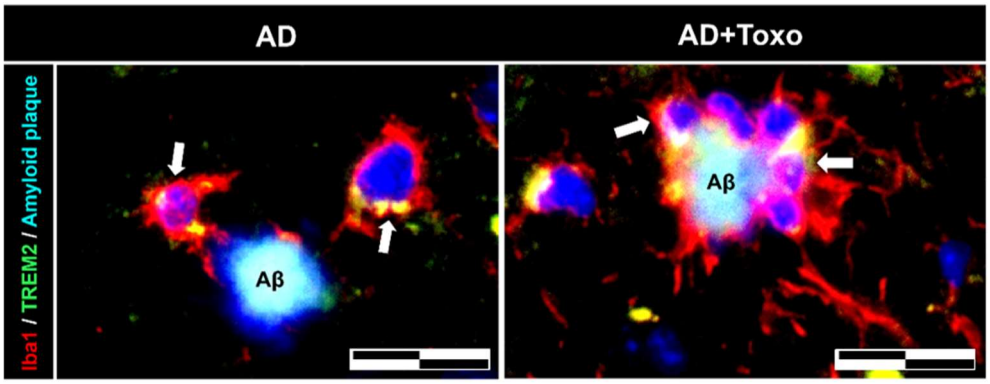


**Figure 2.16. Plaque-associated microglia were shifted to the DAM phenotype in 5XFAD mouse brains**

Plaque-associated microglia (yellow, due to co-staining with Iba-1 (red) and TREM2 (green) and indicated by an arrow) were gathered around amyloid plaques (light blue). The TREM2 signal is a predictor of the DAM phenotype. Scale bar: 20 μm.

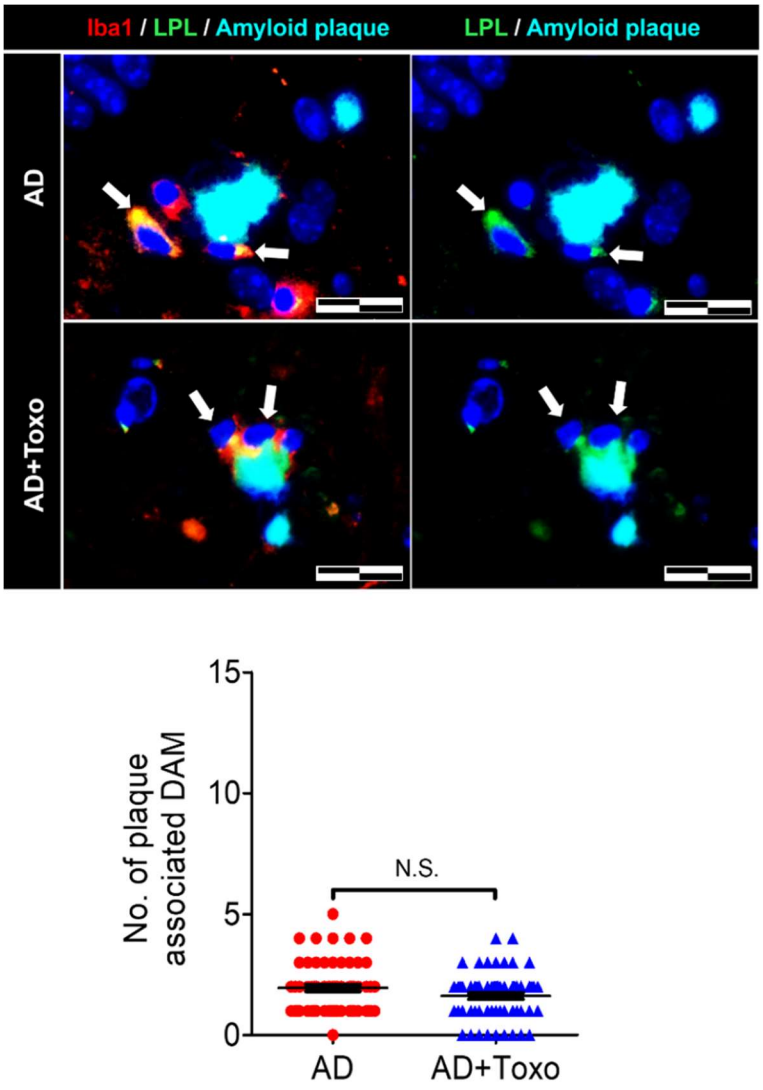


**Figure 2.17. Counting results of plaque-associated DAM microglia in a 5XFAD mouse**

Plaque-associated DAM microglia (yellow, due to co-staining with Iba-1 (red) and LPL (green) and indicated by an arrow). The number of plaque-associated DAM microglial cells found around 60 amyloid plaques distributed in mouse brains (10 randomly selected plaques per mouse × 6 mice per group). Scale bar: 20 μm. Data are presented as mean ± SEM. *Statistical significance compared with the control (* $p < 0.05$).

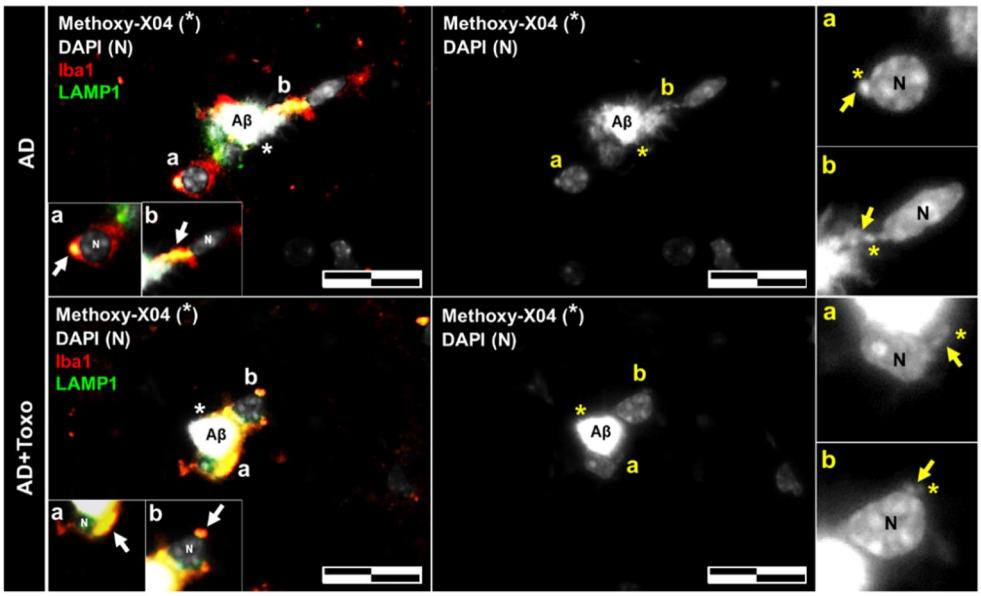


**Figure 2.18. Microglia were capable of removing Aβ plaques with lysosomal degradation in 5XFAD mice**

LAMP1 expression and the colocalization of LAMP1 and Iba1 in microglia around the amyloid β (Aβ) plaque. Lysosomal degradation of Aβ plaque as seen by the internalized puncta per microglial cell. Both "a" and "b" indicate LAMP1 positive lysosomes (white and yellow arrow) with the colocalization of methoxy-X04 stained amyloid β (*). Scale bar: 20 μm.

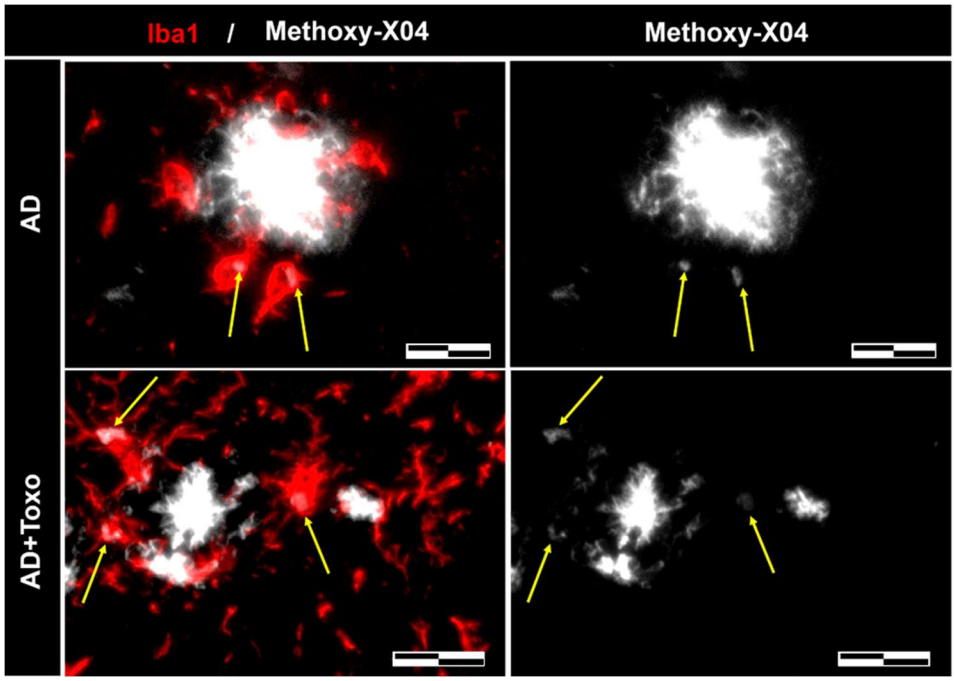


**Figure 2.19. Plaque-associated microglia containing internalized puncta**

Iba-1-stained microglia (red) around methoxy-XO4-stained Aβ plaques (white). Internalized puncta per microglial cell indicates lysosomal degradation of the Aβ plaque (yellow arrow). Scale bar: 20 μm.

**Plaque-associated microglia apoptosis after phagocytosing the Aβ plaque**

The phenomena that microglia shifted to the DAM phenotype after phagocytosing Aβ plaques suggest that it may induce fatal cell changes, such as cell death, in microglia. Therfore, I went on and investigated whether microglia undergo TUNEL+-apoptotic cell death after phagocytosing Aβ plaques (Figure 2.20). TUNEL+-cells were shown in green, and microglial nuclei were shown in blue. Co-staining with TUNEL and DAPI was shown in light blue/white (arrow) and was detected through the fragmented DNA morphology in the nucleus (Figure 2.20). The ratio of apoptotic microglia among plaque-associated microglia was almost 80% in both the AD and AD + Toxo groups (Figure 2.20). Thus, the plaque-associated microglia in both the AD and AD + Toxo groups were apoptosed after phagocytosing Aβ plaques. Graphical abstracts of this study are shown to describe all the results, briefly (Figure 2.21, 2.22).

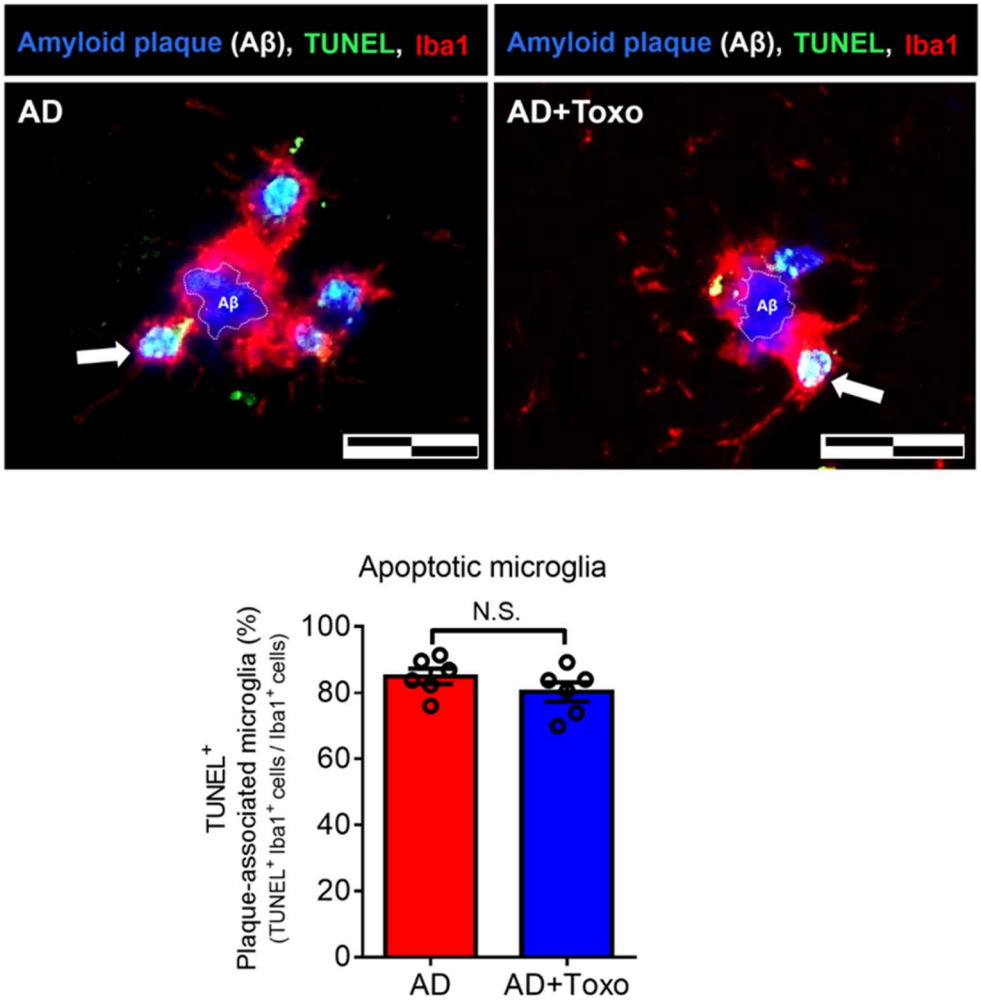


**Figure 2.20. Apoptosis of plaque-associated microglia**

TUNEL+-microglial cells surrounding the Aβ plaque. Arrows represent Iba1 and TUNEL double-positive cells (light blue). The number of Iba1 and TUNEL double-positive cells in plaque-associated microglia. The counting result of plaque-associated apoptotic microglia found around 60 amyloid plaques (10 randomly selected plaques per mouse × 6 mice per group). Scale bar: 20 μm. Data are presented as mean ± SEM.

**Figure 2.21. Graphical abstract of the study**

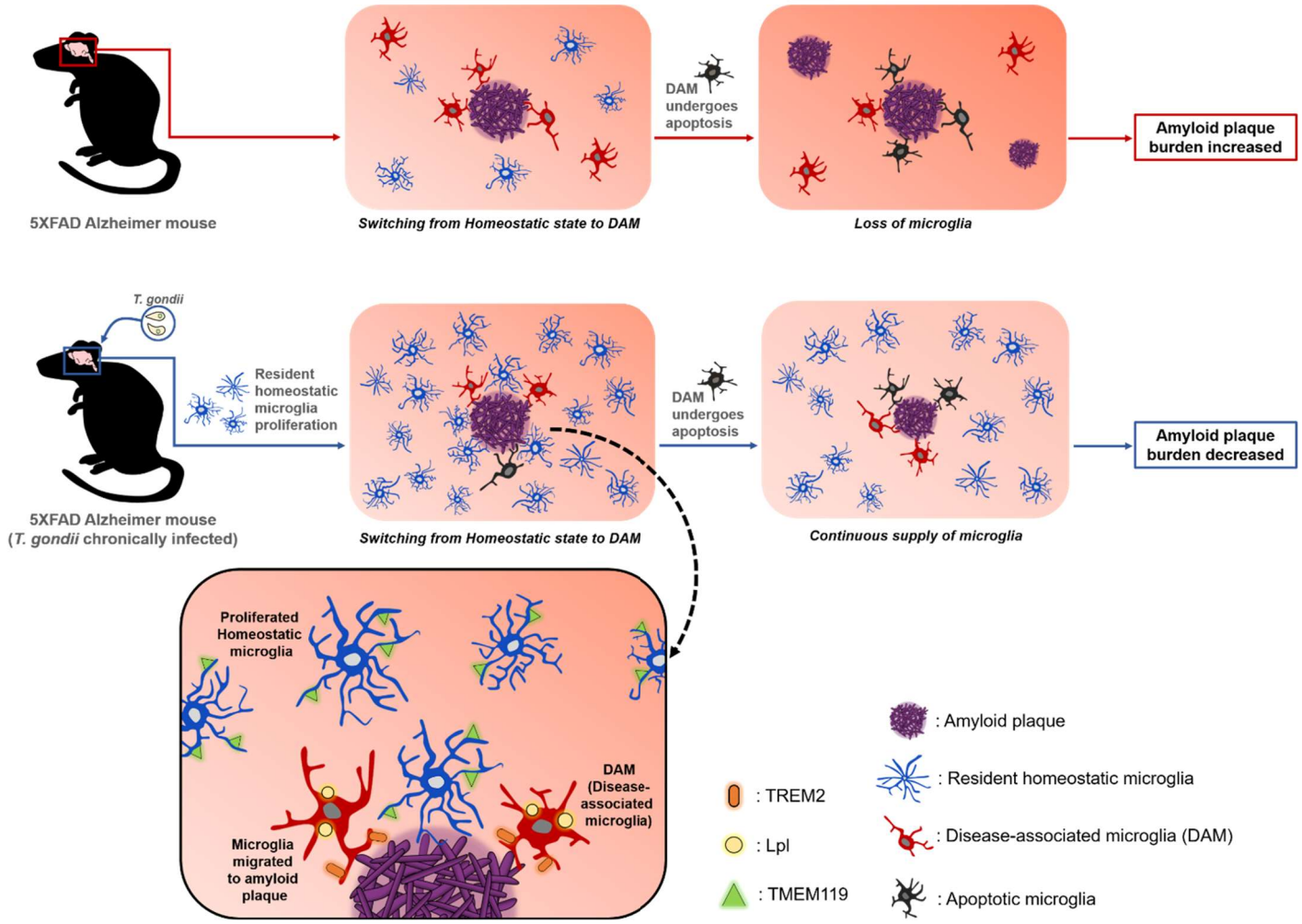

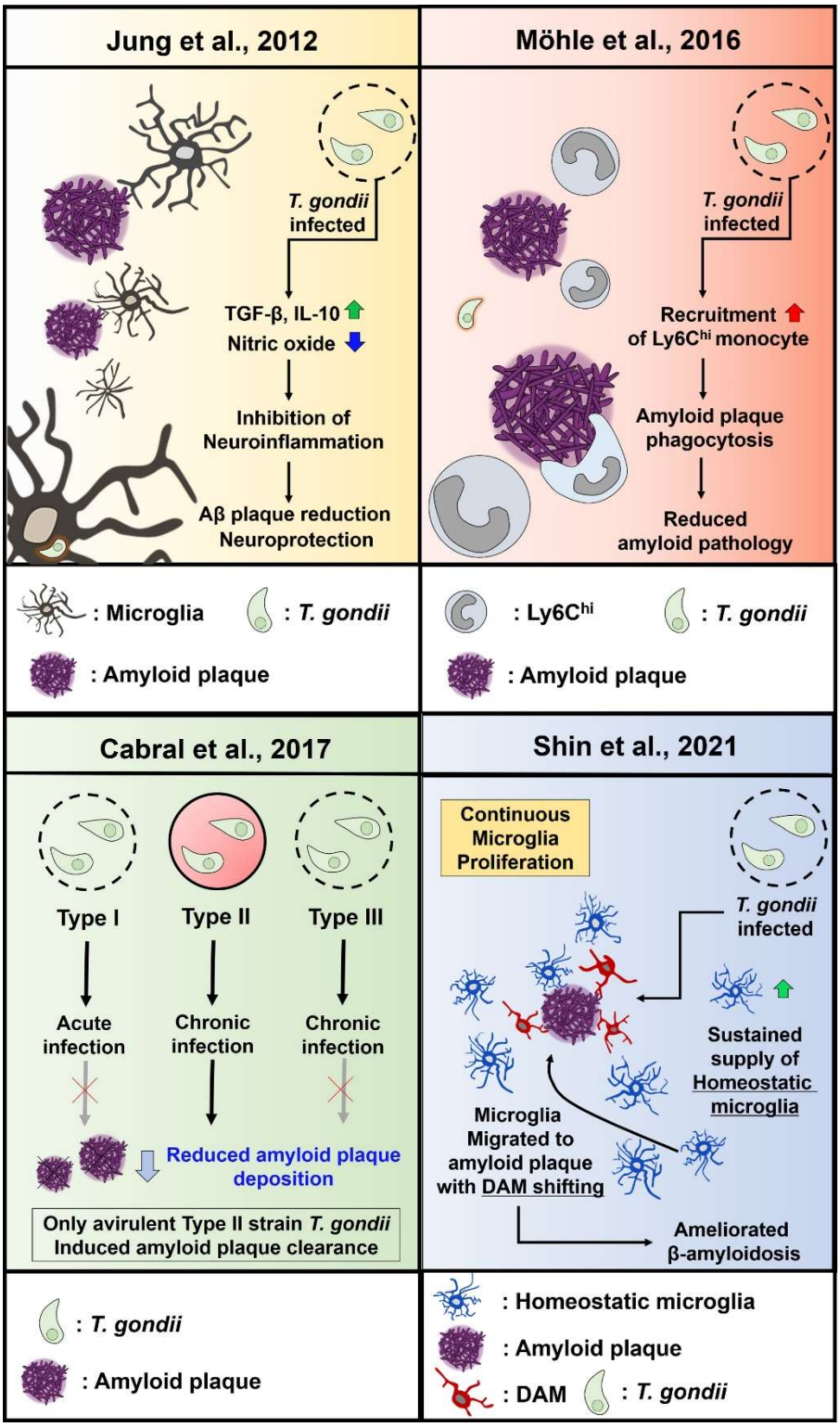


**Figure 2.22. Graphical summary of previous studies and this study about *T. gondii* induced amyloid plaque clearance in AD transgenic mouse model**

**Table 1. Primer sequence**

| Purpose | Gene | Forward primer (5' - 3') | Reverse primer (5' - 3') |
|---|---|---|---|
| Genotyping | APP | AGG ACT GAC CAC TCG ACC AG | CGG GGG TCT AGT TCT GCA T |
| | PSEN1 | AAT AGA GAA CGG CAG GAG CA | GCC ATG AGG GCA CTA ATC AT |
| qRT-PCR | Cst7 | ACA TGC CAG TGG GTC ATC AG | TGC ACG TGC TCC AGT AAT GT |
| | Tmem119 | CAG CAC CCG CAC TGG AAA ATA | CAC CCG TTG GCT TCT AGT CTA |
| | GAPDH | CAT GGC CTC CAA GGA GTA AG | CCT AGG CCC CTC CTG TTA TT |

**Table 2. Antibodies used in IHC, IF staining**

| **Primary antibody** | | |
|---|---|---|
| **Antibody** | **Cat. No.** | **Company** |
| Goat anti-Iba1 antibody | ab5076 | Abcam |
| Rabbit anti-Iba-1 antibody | 019-19741 | FUJIFILM Wako Pure Chemical Corporation |
| Chicken anti-TMEM119 antibody | 400 006 | Synaptic Systems |
| Rat anti-CD11b antibody | MAB1387Z | EMD Millipore |
| Rat anti-Ly6C antibody | ab15627 | Abcam |
| Rat anti-TREM2 antibody | MAB17291 | R&D Systems |
| Rabbit anti-LPL antibody | PA5-85126 | Invitrogen |
| Rabbit anti-LAMP1 antibody | ab24170 | Abcam |
| | | |
| **Secondary antibody** | | |
| **Antibody** | **Cat. No.** | **Company** |
| Rabbit anti-Goat IgG Alexa Fluor® 647 | A21446 | Invitrogen |
| UltraMap anti-Rabbit HRP | 760-4315 | Ventana Medical Systems |
| Goat Anti-Chicken IgY Alexa Fluor® 647 | 103-605-155 | Jackson ImmunoResearch |
| Goat anti-Rat IgG Alexa Fluor® 488 | A11006 | Invitrogen |
| Donkey anti-Goat IgG Alexa Fluor® 568 | A11057 | Invitrogen |
| Donkey anti-Chicken IgY Alexa Fluor® 488 | 703-545-155 | Jackson ImmunoResearch |
| Goat anti-Rat IgG Dylight® 488 | A110-105D2 | Bethyl Laboratories |
| Donkey anti-Rabbit IgG Alexa Fluor® 488 | A21206 | Invitrogen |

# DISCUSSION

Therapies for AD include targeting Aβ plaque formation, neurofibrillary tangle formation, and neuroinflammation (Davies and Koppel, 2009). However, based on results from investigating mechanism-based treatments for AD, the questions of which of the targeted processes are critical for disease progression and how best to inhibit AD remain controversial (Davies and Koppel, 2009). Rational translational research reveals that molecular targeting for treating AD includes using inhibitors against amyloid aggregation, β-secretase, and γ-secretase (Dong et al., 2019; Davies and Koppel, 2009). In addition, antibodies against amyloid (passive immunization); inhibitors of glycogen synthase kinase (GSK)3β, which phosphorylates tau; and nonsteroidal anti-inflammatory drugs (NSAIDs) targeting neuroinflammation can be used as AD treatment (Dong et al., 2019; Davies and Koppel, 2009). However, treatment results have been unsatisfactory (Davies and Koppel, 2009). In recent years, embryonic stem cells, brain-derived neural stem cells, and induced pluripotent stem cells have been used as cell therapy for AD; however, problems persist, including the requirements for a neurosurgical procedure and immunosuppression and tumor formation (Liu et al., 2020). As a novel therapeutic strategy for AD, a nano-based drug delivery system has been suggested (Derakhshankhah et al., 2020).

Despite extensive efforts, treating AD clinically has remained a challenge. The important thing is to consider the multifactorial character of AD, and the development of a single drug is unlikely to lead to universal AD therapy (Derakhshankhah et al., 2020). In sum, the development of alternative therapies is needed to suppress all AD complications by anticipating the intrinsic role of cells

with long-term functions in the brain (Derakhshankhah et al., 2020; Fakhoury, 2018; Hemonnot et al., 2019).

Glial targets were introduced as an implicative strategy for effective AD therapy (Fakhoury, 2018). However, glial-mediated inflammation is a "double-edged sword," performing both detrimental and beneficial functions in AD (Fakhoury, 2018; Hemonnot et al., 2019). In other words, although it is still debatable whether the glial-mediated inflammatory response in AD is a consequence or cause of neurodegeneration, regarding immune surveillance, microglia, as resident macrophages, can preferentially provide the beneficial functions of immunological first defense against invading pathogens and other types of brain injury (Fakhoury, 2018; Hemonnot et al., 2019). Studies have demonstrated the presence of activated microglia at sites of Aβ deposition, suggesting that glial cells interact with Aβ plaques and regulate plaque levels in the brain (Fakhoury, 2018; Blume et al., 2018; Rivera-Escalera et al., 2019). A recent study suggested that most plaque-associated myeloid cells responsible for Aβ plaque clearance are resident microglia (Reed-Geaghan et al., 2020).

When AD mice were induced to overexpress IL-1β in the hippocampus through adenoviral transduction, the number of microglia and microglial capacity to facilitate Aβ plaque clearance increased (Rivera-Escalera et al., 2019). Similarly, these findings revealed that *T. gondii* infection induced continuous microglial proliferation in AD mice, resulting in Aβ plaque clearance. Despite large-scale microglial proliferation, no evidence was found that microglial proliferation increased the number of pyramidal neurons associated with neurodegeneration in the brain tissue

of the AD + Toxo group. Inflammation may be the key neuropathological event leading to neurodegeneration in AD (Fakhoury, 2018). Therefore, the activation of glia, microglia, and astrocytes plays an important role in inducing the inflammatory signaling pathway during neurodegeneration (Fakhoury, 2018). By contrast, although *T. gondii* infection induced M1 polarization and microglial proliferation during 12 weeks of chronic brain infection, a significant induction of inflammatory responses was not observed (Hwang et al., 2018). In this study, microglial proliferation was visualized histologically during the 36-week chronic *T. gondii* infection period, which was molecularly supported by $Ki67^{+}$-mitosis and trophic factor gene expression, indicating the presence of newly dividing homeostatic microglia. Regarding the inflammatory response, although inflammatory cytokines and inflammatory immune responses were not analyzed, ~~a~~ result from the previous studies revealed that the increase of SOCS1 and Arginase1 and the decrease of pSTAT1 and nitric oxide were negative regulators of toxoplasmic encephalitis (Hwang et al., 2018). Therefore, *T. gondii* infection is a new model that proves the beneficial effect of microglia on AD progression.

TREM2 expression in plaque-associated microglia is required for microglia-mediated Aβ phagocytosis (Hemonnot et al., 2019). In this study, the appearance of TREM2-positive microglia around Aβ plaques and the increase in lysosomal digestion of Aβ plaques were related to Aβ clearance in the AD + Toxo group. However, because the fate of the DAM-switched microglia interacting with Aβ was cell death, the presence of stimuli, such as *T. gondii*, which continuously influence the proliferation of homeostatic microglia, is an important factor for Aβ clearance,

as seen for the AD + Toxo group. In other words, it seems evident that an increased number of homeostatic microglia underwent cell death after migrating from the periphery to the plaque border. These results are supported by the microglial turnover rate (newly appearing cells after the disappearance of microglial cells), which increased in AD mice in the presence of amyloid lesions compared with WT mice (Füger et al., 2017).

This study highlights that microglial proliferation was followed up for 36 weeks after *T. gondii* infection. Considering that chronic *T. gondii* infection is defined from approximately 8–9 weeks after infection and the infection state is maintained over a lifelong period, this study is significant in its evaluation of the proliferation kinetics of microglia over a long period after infection (Hwang et al., 2018; Möhle et al., 2016; Derouin and Garin, 1991). Most proliferated microglia were $TMEM119^{+}$/$Iba\text{-}1^{+}$-stained homeostatic microglia, and both plaque-associated and plaque-free microglia were increased in the AD + Toxo group compared with the AD group.

In AD mice, microglia migrate to amyloid plaques, phagocytose the amyloid plaques, and undergo apoptosis after lysosomal degradation of Aβ (Fakhoury, 2018; Klegeris, 2020; Reed-Geaghan et al., 2009; Bolmont et al., 2008). Microglial participation in Aβ degradation is also explained by microglial activation, triggered by highly expressed pattern recognition receptors, including CD14, CD36, and toll-like receptors on the microglial surface (Fakhoury, 2018; Bolmont et al., 2008). My results in this study are in line with that, microglia functioned as neuroprotective cells, clearing the pathological Aβ aggregates through lysosomal degradation. This suggestion is supported by previous data obtained from behavioral studies using

Morris' water maze, where AD mice infected with *T. gondii* (AD + Toxo group) exhibited amelioration of symptoms of loss of cognitive function. By contrast, Green and colleagues reported that microglial depletion impairs parenchymal plaque development (Spangenberg et al., 2019). When microglia, which depend on colony-stimulating factor 1 receptor (CSF1R) signaling for survival, were treated with a CSF1R inhibitor, their population was depleted, and plaques failed to form in the parenchymal space (Spangenberg et al., 2019). The authors asserted that microglia play a role in the onset and development of AD pathology (Spangenberg et al., 2019). However, considering that microglia maintain homeostasis in the brain and play various roles, such as adult neurogenesis and neuronal circuit formation (Chen and Trapp, 2016; Galloway et al., 2019; Laura and Limatola, 2020; Ueno and Yamashita, 2014), it is reasonable to think that microglial depletion plays a role in eliminating the non-resolving inflammatory response during AD pathogenesis. However, whether this depletion is sufficient to prevent AD progression sustainably is debatable. In this context, this study highlights the role of microglia in inhibiting AD progression. In other words, these findings suggest that the characteristics of immunity induced by *T. gondii* infection, namely the simultaneous increase in homeostatic microglia and the suppression of inflammatory immunity, are essential to inhibit the progression of AD. This immune environment induces an increase in microglial Aβ phagocytosis while suppressing the non-resolving inflammatory response in the brain.

Regarding the clearance of Aβ in *T. gondii*-infected 5XFAD mice, in a study by Möhle et al. (2016), Ly6C$^{hi}$ monocytes were associated with increased phagocytosis

and the degradation of soluble Aβ. However, in that study, Iba1-labeled microglia interacted more closely with plaques, but Ly6C$^{hi}$ monocytes did not; histological analysis of *T. gondii*-infected brains also exhibited proliferation and the activation of resident microglia. Nevertheless, that study concluded that Ly6C$^{hi}$ monocytes had more phagocytic capacity than microglia when evaluated for their ability to phagocytose Aβ42 in an *ex vivo* phagocytosis assay specifically and insisted that chronic *T. gondii* infection enhances β-amyloid phagocytosis and clearance by recruited monocytes (Möhle et al., 2016). The most significant difference is the infection period of *T. gondii,* comparing with the above study. In the above research, 5XFAD mice were euthanized at eight weeks after infecting 8-week-old mice with *T. gondii*, while in this study, mice were sacrificed at 40 weeks after infecting 8-week-old mice with *T. gondii*. With the passage of *T. gondii* infection time, the early inflammatory immune response is gradually converted to an anti-inflammatory immune response, and the acute *T. gondii* infection becomes a chronic infection (Jung et al., 2012; Hwang et al., 2018). The early inflammatory response of *T. gondii* in the brain results in the infiltration of Ly6C$^{+}$ monocytes in the brain; however, chronic *T. gondii* infection exhibited an increase in the microglial population (Möhle et al., 2016; Ham et al., 2020; Cabral et al., 2017; Kratofil et al., 2017). Therefore, in this study, the interaction between microglia and Aβ and the reduction of amyloid burden in chronic *T. gondii* infection suggests that microglia are effective inhibitors of Aβ deposition.

Taken together, *T. gondii* infection induced the proliferation of homeostatic microglia during chronic infection, and the number of plaque-associated microglia

in *T. gondii*-infected AD mice was significantly increased compared with uninfected AD mice. Considering that plaque-associated microglia undergo apoptosis after phagocytosing Aβ plaques, the continuous increase in the number of microglia during *T. gondii* infection may be an important factor in reducing Aβ deposition. Notably, the results from a previous study revealed that neuroinflammation and neurodegeneration were not induced during chronic *T. gondii* infection even after microglial proliferation. Therefore, the highlight of this study is to suggest that the therapeutic targets for AD should include both the continuous increasing of microglia and decreasing neuroinflammation in the brain. In this study, I newly demonstrated the potential of *T. gondii* in maintaining long-term microglial proliferation in the brain.

# REFERENCES


1. Baik SH, Kang S, Son SM, Mook-Jung I. Microglia contributes to plaque growth by cell death due to uptake of amyloid β in the brain of Alzheimer's disease mouse model. Glia. 2016 Dec;64(12):2274-2290. doi: 10.1002/glia.23074. Epub 2016 Sep 23. PMID: 27658617.
2. Bennett ML, Bennett FC, Liddelow SA, Ajami B, Zamanian JL, Fernhoff NB, Mulinyawe SB, Bohlen CJ, Adil A, Tucker A, Weissman IL, Chang EF, Li G, Grant GA, Hayden Gephart MG, Barres BA. New tools for studying microglia in the mouse and human CNS. Proc Natl Acad Sci U S A. 2016 Mar 22;113(12):E1738-46. doi: 10.1073/pnas.1525528113. Epub 2016 Feb 16. PMID: 26884166; PMCID: PMC4812770.
3. Blume T, Focke C, Peters F, Deussing M, Albert NL, Lindner S, Gildehaus FJ, von Ungern-Sternberg B, Ozmen L, Baumann K, Bartenstein P, Rominger A, Herms J, Brendel M. Microglial response to increasing amyloid load saturates with aging: a longitudinal dual tracer in vivo μPET-study. J Neuroinflammation. 2018 Nov 6;15(1):307. doi: 10.1186/s12974-018-1347-6. PMID: 30400912; PMCID: PMC6220478.
4. Bolmont T, Haiss F, Eicke D, Radde R, Mathis CA, Klunk WE, Kohsaka S, Jucker M, Calhoun ME. Dynamics of the microglial/amyloid interaction indicate a role in plaque maintenance. J Neurosci. 2008 Apr 16;28(16):4283-92. doi: 10.1523/JNEUROSCI.4814-07.2008. PMID: 18417708; PMCID: PMC3844768.
5. Cabral CM, McGovern KE, MacDonald WR, Franco J, Koshy AA.

Dissecting amyloid beta deposition using distinct strains of the neurotropic parasite *Toxoplasma gondii* as a novel tool. ASN Neuro. 2017 Jul-Aug;9(4):1759091417724915. doi: 10.1177/1759091417724915. PMID: 28817954; PMCID: PMC5565021.

6. Chen Z, Trapp BD. Microglia and neuroprotection. J Neurochem. 2016 Jan;136 Suppl 1:10-7. doi: 10.1111/jnc.13062. Epub 2015 Mar 10. PMID: 25693054.
7. Davies P, Koppel J. Mechanism-based treatments for Alzheimer's disease. Dialogues Clin Neurosci. 2009;11(2):159-69. doi: 10.31887/DCNS.2009.11.2/pdavies. PMID: 19585951; PMCID: PMC2905040.
8. Deczkowska A, Keren-Shaul H, Weiner A, Colonna M, Schwartz M, Amit I. Disease-associated microglia: A universal immune sensor of neurodegeneration. Cell. 2018 May 17;173(5):1073-1081. doi: 10.1016/j.cell.2018.05.003. PMID: 29775591.
9. Derakhshankhah H, Sajadimajd S, Jafari S, Izadi Z, Sarvari S, Sharifi M, Falahati M, Moakedi F, Muganda WCA, Müller M, Raoufi M, Presley JF. Novel therapeutic strategies for Alzheimer's disease: Implications from cell-based therapy and nanotherapy. Nanomedicine. 2020 Feb;24:102149. doi: 10.1016/j.nano.2020.102149. Epub 2020 Jan 10. PMID: 31927133.
10. Derouin F, Garin YJ. *Toxoplasma gondii*: blood and tissue kinetics during acute and chronic infections in mice. Exp Parasitol. 1991 Nov;73(4):460-8. doi: 10.1016/0014-4894(91)90070-d. PMID: 1959573.

11. Dong Y, Li X, Cheng J, Hou L. Drug development for Alzheimer's disease: microglia induced neuroinflammation as a target? Int J Mol Sci. 2019 Jan 28;20(3):558. doi: 10.3390/ijms20030558. PMID: 30696107; PMCID: PMC6386861.
12. Fakhoury M. Microglia and astrocytes in Alzheimer's disease: Implications for therapy. Curr Neuropharmacol. 2018;16(5):508-518. doi: 10.2174/1570159X15666170720095240. PMID: 28730967; PMCID: PMC5997862.
13. Frost JL, Schafer DP. Microglia: Architects of the developing nervous system. Trends Cell Biol. 2016 Aug;26(8):587-597. doi: 10.1016/j.tcb.2016.02.006. Epub 2016 Mar 20. PMID: 27004698; PMCID: PMC4961529.
14. Füger P, Hefendehl JK, Veeraraghavalu K, Wendeln AC, Schlosser C, Obermüller U, Wegenast-Braun BM, Neher JJ, Martus P, Kohsaka S, Thunemann M, Feil R, Sisodia SS, Skodras A, Jucker M. Microglia turnover with aging and in an Alzheimer's model via long-term in vivo single-cell imaging. Nat Neurosci. 2017 Oct;20(10):1371-1376. doi: 10.1038/nn.4631. Epub 2017 Aug 28. PMID: 28846081.
15. Galloway DA, Phillips AEM, Owen DRJ, Moore CS. Phagocytosis in the brain: Homeostasis and disease. Front Immunol. 2019 Apr 16;10:790. doi: 10.3389/fimmu.2019.00790. Erratum in: Front Immunol. 2019 Jul 10;10:1575. PMID: 31040847; PMCID: PMC6477030.
16. Ginhoux F, Garel S. The mysterious origins of microglia. Nat Neurosci.

2018 Jul;21(7):897-899. doi: 10.1038/s41593-018-0176-3. PMID: 29942037.

17. Griciuc A, Tanzi RE. The role of innate immune genes in Alzheimer's disease. Curr Opin Neurol. 2021 Apr 1;34(2):228-236. doi: 10.1097/WCO.0000000000000911. PMID: 33560670; PMCID: PMC7954128.
18. Ham DW, Kim SG, Seo SH, Shin JH, Lee SH, Shin EH. Chronic *Toxoplasma gondii* infection alleviates experimental autoimmune encephalomyelitis by the immune regulation inducing reduction in IL-17A/Th17 via upregulation of SOCS3. Neurotherapeutics. 2020 Nov 17. doi: 10.1007/s13311-020-00957-9. Epub ahead of print. PMID: 33205383.
19. Hemonnot AL, Hua J, Ulmann L, Hirbec H. Microglia in Alzheimer disease: Well-known targets and new opportunities. Front Aging Neurosci. 2019 Aug 30;11:233. doi: 10.3389/fnagi.2019.00233. PMID: 31543810; PMCID: PMC6730262.
20. Hwang YS, Shin JH, Yang JP, Jung BK, Lee SH, Shin EH. Characteristics of infection immunity regulated by *Toxoplasma gondii* to maintain chronic infection in the brain. Front Immunol. 2018 Feb 5;9:158. doi: 10.3389/fimmu.2018.00158. PMID: 29459868; PMCID: PMC5807351.
21. Jung BK, Pyo KH, Shin KY, Hwang YS, Lim H, Lee SJ, Moon JH, Lee SH, Suh YH, Chai JY, Shin EH. *Toxoplasma gondii* infection in the brain inhibits neuronal degeneration and learning and memory impairments in a murine model of Alzheimer's disease. PLoS One. 2012;7(3):e33312. doi:

10.1371/journal.pone.0033312. Epub 2012 Mar 21. PMID: 22470449; PMCID: PMC3310043.

22. Keren-Shaul H, Spinrad A, Weiner A, Matcovitch-Natan O, Dvir-Szternfeld R, Ulland TK, David E, Baruch K, Lara-Astaiso D, Toth B, Itzkovitz S, Colonna M, Schwartz M, Amit I. A unique microglia type associated with restricting development of Alzheimer's disease. Cell. 2017 Jun 15;169(7):1276-1290.e17. doi: 10.1016/j.cell.2017.05.018. Epub 2017 Jun 8. PMID: 28602351.
23. Klegeris A. Microglial targets for effective therapies of Alzheimer's disease. Front Drug Chem Clin Res. 2020 Mar; 3:1–4. doi: 10.15761/FDCCR.1000145
24. Kratofil RM, Kubes P, Deniset JF. Monocyte conversion during inflammation and injury. Arterioscler Thromb Vasc Biol. 2017 Jan;37(1):35-42. doi: 10.1161/ATVBAHA.116.308198. Epub 2016 Oct 20. PMID: 27765768.
25. Lauro C, Limatola C. Metabolic reprograming of microglia in the regulation of the innate inflammatory response. Front Immunol. 2020 Mar 20;11:493. doi: 10.3389/fimmu.2020.00493. PMID: 32265936; PMCID: PMC7099404.
26. Lee JE, Han PL. An update of animal models of Alzheimer disease with a reevaluation of plaque depositions. Exp Neurobiol. 2013 Jun;22(2):84-95. doi: 10.5607/en.2013.22.2.84. Epub 2013 Jun 27. PMID: 23833557; PMCID: PMC3699678.

27. Liu XY, Yang LP, Zhao L. Stem cell therapy for Alzheimer's disease. World J Stem Cells. 2020 Aug 26;12(8):787-802. doi: 10.4252/wjsc.v12.i8.787. PMID: 32952859; PMCID: PMC7477654.

28. Möhle L, Israel N, Paarmann K, Krohn M, Pietkiewicz S, Müller A, Lavrik IN, Buguliskis JS, Schott BH, Schlüter D, Gundelfinger ED, Montag D, Seifert U, Pahnke J, Dunay IR. Chronic *Toxoplasma gondii* infection enhances β-amyloid phagocytosis and clearance by recruited monocytes. Acta Neuropathol Commun. 2016 Mar 16;4:25. doi: 10.1186/s40478-016-0293-8. PMID: 26984535; PMCID: PMC4793516.

29. Oakley H, Cole SL, Logan S, Maus E, Shao P, Craft J, Guillozet-Bongaarts A, Ohno M, Disterhoft J, Van Eldik L, Berry R, Vassar R. Intraneuronal beta-amyloid aggregates, neurodegeneration, and neuron loss in transgenic mice with five familial Alzheimer's disease mutations: potential factors in amyloid plaque formation. J Neurosci. 2006 Oct 4;26(40):10129-40. doi: 10.1523/JNEUROSCI.1202-06.2006. PMID: 17021169; PMCID: PMC6674618.

30. Rangaraju S, Dammer EB, Raza SA, Rathakrishnan P, Xiao H, Gao T, Duong DM, Pennington MW, Lah JJ, Seyfried NT, Levey AI. Identification and therapeutic modulation of a pro-inflammatory subset of disease-associated-microglia in Alzheimer's disease. Mol Neurodegener. 2018 May 21;13(1):24. doi: 10.1186/s13024-018-0254-8. PMID: 29784049; PMCID: PMC5963076.

31. Reed-Geaghan EG, Croxford AL, Becher B, Landreth GE. Plaque-

associated myeloid cells derive from resident microglia in an Alzheimer's disease model. J Exp Med. 2020 Apr 6;217(4):e20191374. doi: 10.1084/jem.20191374. PMID: 31967645; PMCID: PMC7144522.

32. Reed-Geaghan EG, Savage JC, Hise AG, Landreth GE. CD14 and toll-like receptors 2 and 4 are required for fibrillar A{beta}-stimulated microglial activation. J Neurosci. 2009 Sep 23;29(38):11982-92. doi: 10.1523/JNEUROSCI.3158-09.2009. PMID: 19776284; PMCID: PMC2778845.
33. Rivera-Escalera F, Pinney JJ, Owlett L, Ahmed H, Thakar J, Olschowka JA, Elliott MR, O'Banion MK. IL-1β-driven amyloid plaque clearance is associated with an expansion of transcriptionally reprogrammed microglia. J Neuroinflammation. 2019 Dec 10;16(1):261. doi: 10.1186/s12974-019-1645-7. PMID: 31822279; PMCID: PMC6902486.
34. Shin JH, Hwang YS, Jung BK, Seo SH, Ham DW, Shin EH. Reduction of amyloid burden by proliferated homeostatic microglia in *Toxoplasma gondii*-infected Alzheimer's disease model mice. Int J Mol Sci. 2021 Mar 9;22(5):2764. doi: 10.3390/ijms22052764. PMID: 33803262.
35. Sobue A, Komine O, Hara Y, Endo F, Mizoguchi H, Watanabe S, Murayama S, Saito T, Saido TC, Sahara N, Higuchi M, Ogi T, Yamanaka K. Microglial gene signature reveals loss of homeostatic microglia associated with neurodegeneration of Alzheimer's disease. Acta Neuropathol Commun. 2021 Jan 5;9(1):1. doi: 10.1186/s40478-020-01099-x. PMID: 33402227; PMCID: PMC7786928.

36. Spangenberg E, Severson PL, Hohsfield LA, Crapser J, Zhang J, Burton EA, Zhang Y, Spevak W, Lin J, Phan NY, Habets G, Rymar A, Tsang G, Walters J, Nespi M, Singh P, Broome S, Ibrahim P, Zhang C, Bollag G, West BL, Green KN. Sustained microglial depletion with CSF1R inhibitor impairs parenchymal plaque development in an Alzheimer's disease model. Nat Commun. 2019 Aug 21;10(1):3758. doi: 10.1038/s41467-019-11674-z. PMID: 31434879; PMCID: PMC6704256.

37. Ueno M, Yamashita T. Bidirectional tuning of microglia in the developing brain: from neurogenesis to neural circuit formation. Curr Opin Neurobiol. 2014 Aug;27:8-15. doi: 10.1016/j.conb.2014.02.004. Epub 2014 Mar 5. PMID: 24607651.

38. Wes PD, Sayed FA, Bard F, Gan L. Targeting microglia for the treatment of Alzheimer's Disease. Glia. 2016 Oct;64(10):1710-32. doi: 10.1002/glia.22988. Epub 2016 Apr 21. PMID: 27100611.

# 초 록

알츠하이머병은 뇌내 아밀로이드 플라크의 축적과 함께 점진적으로 악화되는 병으로 알려져 있다. 최근 연구에 따르면, 만성 톡소포자충 감염이 알츠하이머병 모델 마우스에서 아밀로이드 플라크 부하를 감소시키며, 관련 기전으로 톡소포자충에 의해 유도된 항염증성 사이토카인(전환성장인자 베타 및 인터루킨-10)의 방출과, 높아진 Ly6C$^{hi}$ 단핵구 수치가 아밀로이드 플라크 부하 감소의 원인이 될 수 있음이 제시되었다. 미세아교세포의 포식 작용도 알츠하이머병에서 아밀로이드 플라크를 제거하는데 중요하다는 것은 잘 알려져 있지만, 최근까지도 톡소포자충에 감염된 후 미세아교세포의 증식과 아밀로이드 플라크 부하 감소 및 알츠하이머병 병리와의 기전적 연관성에 대해서는 확실히 알려진바가 없다. 본 연구의 목적은, 5XFAD 형질 전환 마우스를 사용하여 아밀로이드 플라크 감소에 대한 미세 아교 세포 증식 및 표현형 변화에서 톡소포자충 감염의 역할을 분석하고 그 결과를 대조군과 비교하는 것이다.

연구결과, 일반 마우스의 뇌에서 톡소포자충 감염 3주에서 36주 동안, Iba1-양성의 미세아교세포 및 TMEM119-양성의 뇌내 거주 항상성 미세아교세포의 수가 증식마커인 Ki67의 발현을 동반하며 유의성 있게 증가하였다. 마이크로어레이 분석 상의 미세아교세포 마커 (*Iba1*, *P2ry13*, *Cx3cr1*, *Tmem119*)와 영양인자 (*Il1β*, *Tnfα*, *Mcsf*, *NFκB1*)도 미세아교세포의 증식과 일치하는 결과를 보였다. 이후 5XFAD 알츠하이머병 모델 마우스군 (AD 실험군)과 톡소포자충을 감염시킨 실험군 (AD+Toxo 실험군)에서 회수한 뇌 조직을 이용하여 미세아교세포의 증식과 아밀로이드 베타 플라크 부하 간의 상관관계를 분석하였다. 톡소포자충 감염

10개월 후, AD+Toxo 실험군은 AD 실험군에 비해 아밀로이드 플라크 부하가 유의하게 감소하였고, 그에 반해 항상성 미세아교세포의 수와 플라크 인접 미세아교세포의 수는 유의하게 증가하였다. 마이크로어레이 분석 상의 미세아교세포 마커 (*Iba1*, *P2ry13*, *Cx3cr1*, *Tmem119*)와 영양인자 (*Il1β*, *Tnfα*, *Mcsf*, *NFκB1*)는 AD+Toxo 실험군에서 증가하였으며, Aβ 펩타이드의 효소결합면역흡착검사 결과는 아밀로이드 플라크 계수 결과와 같이 AD+Toxo 실험군에서 유의성 있게 감소하는 것으로 나타났다. 대부분의 플라크 인접 미세아교세포는 AD 실험군과 AD+Toxo 실험군 모두에서 TREM2와 Lpl을 발현하는 질병연관 미세아교세포로 표현형이 분화되는 것을 확인하였고, 동시에 플라크 인접 미세아교세포 대부분이 아밀로이드 베타 플라크를 포식 및 분해하는 과정에서 세포자멸사를 겪는 것으로 확인되었다. 이는 항상성 미세아교세포의 지속적인 공급이 아밀로이드 베타 플라크 부하의 감소에 필수적이라는 것을 확실하게 시사해준다.

본 연구를 통해 만성의 톡소포자충 감염이 진행성 알츠하이머병 마우스의 뇌 내 미세아교세포의 증식을 유도할 수 있음을 발견할 수 있었고, 그로 인한 항상성 미세아교세포의 지속적인 공급이 향후 알츠하이머병에 대한 치료전략이 될 수 있음을 확인할 수 있었다.

**주요어:** 톡소포자충, 만성 감염, 항상성 미세아교세포, 알츠하이머병, 5XFAD 마우스, 질병 연관 미세아교세포

**학 번: 2015-21959**